

NASA TECHNICAL NOTE



NASA TN D-4820

C.1

NASA TN D-4820

LOAN COPY: RE
AFWL (WLI
KIRTLAND AFB,

0131719



TECH LIBRARY KAFB, NM

A HOVERING INVESTIGATION OF AN EXTREMELY FLEXIBLE LIFTING ROTOR

by Matthew M. Winston

Langley Research Center

Langley Station, Hampton, Va.



A HOVERING INVESTIGATION OF AN EXTREMELY
FLEXIBLE LIFTING ROTOR

By Matthew M. Winston

Langley Research Center
Langley Station, Hampton, Va.

NATIONAL AERONAUTICS AND SPACE ADMINISTRATION

For sale by the Clearinghouse for Federal Scientific and Technical Information
Springfield, Virginia 22151 - CFSTI price \$3.00

A HOVERING INVESTIGATION OF AN EXTREMELY FLEXIBLE LIFTING ROTOR

By Matthew M. Winston
Langley Research Center

SUMMARY

A hovering investigation of an extremely flexible rotor was conducted to determine the effects of rotor-tip configuration and operating conditions on performance and to obtain a comparison with a conventional rotor.

The results show the manner in which luffing (fabric instability) restricted the envelope of tip speed and collective pitch angles within which the rotor could be operated. In the range where the rotor could be operated, variations in tip speed altered the blade camber and resulted in substantial variations with tip speed in hovering performance, particularly at the higher thrust conditions. The results suggest the existence of optimum combinations of tip body mass, tip center of gravity, and tip stabilizer incidence for each value of tip speed since these variables determine the amount and distribution of blade camber and twist. The hovering efficiency of this rotor was poor in comparison with a conventional rotor. Because of the large amount of aerodynamically induced camber, however, the rotor attained very high mean lift coefficients.

INTRODUCTION

Current interest in extremely flexible lifting rotors arises primarily from their apparent potential to provide lighter rotor weights, stowability, and the capability for in-flight deployment. If the operation of such rotors could be made feasible, they could be used for large load lifting helicopters, booster and reentry vehicle recovery, and convertible aircraft. Of some of the previous flexible rotor studies (refs. 1 to 3) one investigation (ref. 1) included a comparison of the hovering characteristics of a 30-foot-diameter (9.144-meter) flexible-rotor configuration with those of a conventional rotor from reference 4. In comparison, the flexible rotor exhibited much lower hovering efficiency while attaining higher mean lift coefficients than the conventional rotor. Also, the fabric instability, commonly called "luffing," was found to limit severely the envelope of tip speeds and blade pitch settings within which the flexible rotor could be operated.

Therefore, the present investigation was undertaken to determine the effects of variations in the rotor configuration and operating conditions on the hovering performance

of the previously tested flexible rotor. In addition, it was attempted to define the non-luffing envelope of tip speeds and collective pitch angles for a rotor of this type.

SYMBOLS

Units for the physical quantities used herein are presented in both the U.S. Customary System of Units and the International System of Units. Factors relating these two systems of units may be found in reference 5.

b	number of blades, for this investigation 2
c	blade local chord, ft (meters)
c_e	blade equivalent chord, $\frac{\int_0^R cr^2 dr}{\int_0^R r^2 dr}$, 0.777 ft (0.237 meter)
\bar{C}_L	rotor mean lift coefficient, $6 \frac{C_T}{\sigma}$
C_Q	rotor torque coefficient, $\frac{\text{Torque}}{\pi R^2 \rho (\Omega R)^2 R}$
C_T	rotor thrust coefficient, $\frac{\text{Thrust}}{\pi R^2 \rho (\Omega R)^2}$
i_s	tip stabilizer incidence with respect to tip body chord line – positive when trailing edge is down, deg
M	rotor figure of merit, $0.707 \frac{(C_T)^{3/2}}{C_Q}$
r	radial distance to any blade section, ft (meters)
R	rotor radius, ft (meters)
θ_{root}	pitch angle measured at blade root, angle between blade root-chord line and plane perpendicular to rotor shaft, deg
ρ	mass density of air, $\frac{\text{slugs}}{\text{ft}^3}$ $\left(\frac{\text{kilograms}}{\text{meters}^3} \right)$

- σ rotor solidity, $\frac{bc_e}{\pi R}$, 0.0329
- Ω rotational speed, radians/sec

APPARATUS AND TESTS

Apparatus

The rotor used in this investigation has the blade planform shaped so that chordwise and spanwise components of centrifugal force provide most of the blade stiffness during operation. The centrifugal forces are provided by concentrated masses at the blade tips. Pertinent rotor dimensions are given in figure 1 and a photograph of the rotor mounted on the Langley helicopter tower is given in figure 2.

The leading and trailing edges of the blades are high-strength steel rods, and the fabric airfoil is made of low-porosity dacron sailcloth. The mass and chordwise balance of the steel and aluminum tip bodies can be varied by changing small removable weights in the nose section. A horizontal stabilizer is attached at the tip-body aft section. This stabilizer is a solid aluminum NACA 0006 airfoil swept 30° aft with respect to the blade span axis. Its incidence with respect to the tip-body chord line can be varied through ±15° in 5° increments.

Sensors for control positions and motions of each blade were mounted on the rotor hub. Thrust, torque, and rotor-speed transducers were located along the rotor shaft. The outputs from the sensors for one blade were fed to microammeters for monitoring. The outputs from all other sensors were recorded on an oscillograph. High-speed motion pictures were used to assist in evaluating the rotor behavior.

Tests

The rotor was investigated at the Langley helicopter test tower where it was exposed to local wind conditions. Since it was desired to operate as near as possible to zero wind conditions, a recording anemometer was used to monitor wind conditions in the vicinity of the test site.

Three basic configurations were investigated. The differences consisted of changes in tip body mass and chordwise balance and are listed in the following table:

Configuration	Mass, slugs (kg)	Center of gravity, percent of tip chord from leading edge	Tip stabilizer incidence, deg
1	0.295 (4.305)	30.5	-5, -10, -15
2	.311 (4.539)	25.0	-5, -10, -15
3	.326 (4.758)	19.0	-10, -15

Each tip-body configuration was operated through a range of collective pitch angles and tip speeds at each stabilizer setting. Only the negative stabilizer settings were used since preliminary tests indicated that positive settings caused negative tip incidences and would not permit satisfactory operation. The maximum rotor-tip speed was limited to about 320 ft/sec (97.5 m/sec) for structural reasons. Measurements of forces and moments were made at selected pitch angles, and from these data the hovering characteristics were determined.

PRESENTATION OF RESULTS

Individual test points are not shown in the performance data because the coefficients and other dimensionless ratios were computed from faired plots of the basic force and moment data. This procedure was used to minimize the effect of deviations in wind velocity from zero and small fluctuations in the rotor speed. Most of the measurements were made in winds from 0 to 2 miles per hour (0 to 0.9 m/sec); however, at the lowest tip speed, an increase in wind velocity to as little as 5 miles per hour (2.2 m/sec) represented forward flight conditions at a tip-speed ratio of about 0.055.

The principal errors in the data are attributed to the accuracy to which the measurements could be obtained. The magnitudes of the probable errors in $\frac{C_Q}{\sigma}$, $\frac{C_T}{\sigma}$, and C_T are given in figure 3 as a function of tip speed. In addition, the figure of merit, which combines these coefficients, is subject to the probable errors in both the thrust and torque measurements. However, the probable error in figure of merit is not only a function of tip speed but also a function of the magnitude of the force measurements. Therefore, the figure-of-merit variations are presented in all cases as a broad band, the width of the band representing the probable error.

The results of this investigation are presented as follows:

	Figure
Rotor luffing boundaries	4
Basic hovering characteristics:	
Configuration 1:	
$i_S = -5^\circ$	5
$i_S = -10^\circ$	6
$i_S = -15^\circ$	7
Configuration 2:	
$i_S = -5^\circ$	8
$i_S = -10^\circ$	9
$i_S = -15^\circ$	10

	Figure
Configuration 3:	
$i_s = -10^\circ$	11
$i_s = -15^\circ$	12
Tip speed effects, $i_s = -15^\circ$:	
Configuration 1	13
Configuration 2	14
Configuration 3	15
Effects of tip mass and center of gravity:	
$i_s = -5^\circ$, $\Omega R = 220$ ft/sec (67 m/sec).	16
Effects of tip stabilizer incidence:	
Configuration 2, $\Omega R = 220$ ft/sec (67 m/sec)	17
Comparison of flexible rotor with conventional rotor:	
$\Omega R = 310$ ft/sec (94.5 m/sec)	18

RESULTS

Luffing Restrictions

It was not possible to investigate all configurations of the flexible rotor for the same envelope of blade-root pitch angles and tip speeds because of the fabric instability commonly called "luffing." Luffing generally occurs at the lower blade-section angles of attack and is usually considered to result from positive pressures acting on the convex surface of the cambered fabric. Since the rotor blades are free to twist locally, they assume different twist and camber distributions for each change in rotor-tip configuration or tip speed. The twist and camber distributions, in turn, determine the root pitch angle at which some outboard rotor sections are below the luffing boundary.

The variation of minimum nonluffing angle with tip speed is given in figure 4(a) for the three configurations investigated. The symbols indicate the measured root angle below which rotor vibrations attributed to luffing became so severe that further operation was judged to be impractical and possibly damaging to the rotor system. The trend of increasing minimum pitch angle with speed is as previously experienced. (See ref. 1.) The data indicate that this trend is probably the result of increasing rotor inflow angles (and, consequently, diminishing local angles of attack) as tip speed is increased. For example, figure 10(a) shows that at a blade root angle of 14° , the rotor thrust coefficient, and hence the inflow angle, increases with tip speed.

The available data did not indicate stall (that is, a decrease in the slope of the $C_T - \theta_{\text{root}}$ variation at the higher pitch angles) for all configurations, although observation of tuft motion pictures indicated local separation on inboard portions of the blades

over a considerable portion of the operating range in all cases. In order to illustrate both the upper (stall) boundary and lower (luffing) boundary of the rotor operating envelope, data from configuration 2 which did indicate stall throughout the speed range are given in figure 4(b). The operating range for this configuration is as shown. The shape of this luff-free operating envelope is believed to be general for rotors of this type. Differences in configuration and operating conditions can be expected to shift either or both boundaries.

In theory, flexible rotors of the type used for this investigation can be designed so that in the normal range of operation, they are not susceptible to luffing. (See ref. 1.) Logically, for rotors in this category, the luffing boundaries discussed here have no significance.

Effect of Tip Speed

All the basic hovering data (figs. 5 to 12) indicate a significant effect of tip speed on the rotor characteristics. At the lower tip speeds, the figures of merit and mean lift coefficients were generally higher than those attained at the higher speeds. The lower tip speeds, however, were considerably below those speeds considered practical for normal rotor operation. As the tip speed was increased to the highest values of the tests, the rotor performance deteriorated to a point well below that expected for a conventional rotor.

In figures 13, 14, and 15, the variations with tip speed of thrust coefficient, torque coefficient-solidity ratio, and figure of merit are summarized for the three tip-body configurations with $i_g = -15^\circ$. In nearly all cases, the rotor thrust coefficient decreased, and the torque coefficient increased with tip speed. Generally, the rate of change of these quantities with speed was greater at the higher thrust conditions. Comparison of the figure-of-merit variations for the three configurations (figs. 13(c), 14(c), and 15(c)) shows that the effect of rotor speed was different for each tip-body arrangement. Configuration 3 was comparatively more sensitive to speed variations at all mean lift coefficients than configurations 1 and 2 were. These results indicate that the relationship of flexible-rotor performance to tip speed is dependent upon both the tip-body configuration and the blade loading.

Deterioration of rotor hovering performance with increasing tip speed is usually attributed to increased profile drag coefficient resulting from Mach number effects. (See ref. 4, for example.) For this rotor, however, the effect of tip speed on the blade camber and twist is believed to be the predominant cause of increased profile losses. At large lift coefficients, the section lift-drag ratio, at constant lift coefficient, is increased with increases in camber. At low tip speeds, the aerodynamically induced camber of a flexible blade section is large. However, with increased tip speed, the centrifugal forces act to reduce the blade camber and hence reduce the blade section lift-drag ratio.

Tip-Body and Stabilizer Effects

Since the camber is determined by the relationship between the chordwise centrifugal force components and the aerodynamic forces, tip body mass directly determines the amount of camber developed at a given rotor speed. The chordwise center of gravity, inasmuch as it determines the blade twist axis, influences the radial distribution of both twist and camber. The results of the present investigation reflect the effects of both mass and center-of-gravity position in combination, since the center-of-gravity changes were obtained by adding mass ahead of the tip leading edge.

One example of tip-body effects is given in figure 16 where the rotor hovering characteristics of the three tip configurations at a fixed stabilizer setting are presented. The variations in performance effected by varying the tip configuration are significant. The trends shown in figure 16, however, must be considered valid only for that particular stabilizer setting since the stabilizer incidence also affects the blade twist. Other data show that the effects of tip-body changes at other stabilizer settings can be appreciably different from those shown in the present example.

The effects of tip-stabilizer incidence on the hovering performance of configuration 2 (fig. 17) are also considered to be valid only for that specific mass and center-of-gravity location. The differences in performance increments for equal increments in stabilizer angle indicate that each tip body arrangement has an optimum stabilizer setting.

The foregoing results indicate that any variation in either tip mass, tip chordwise center of gravity, or stabilizer setting causes variations in hovering performance by affecting the amount and radial distribution of twist and camber. As shown in a previous section of this paper, these effects are further modified by the influence of tip speed. The determination of optimum combinations of rotor configuration and operating conditions requires further investigation. Aside from tip speed, the location of the tip center of gravity is believed to be one of the more important parameters since it not only affects the aerodynamic performance but also the aeroelastic stability of the flexible rotor. (See refs. 1 to 3.)

Comparison of Flexible Rotor With Conventional Rotor

In figure 18 the hovering characteristics of the rotor used in this investigation are compared with those of a conventional rotor having NACA 0012 airfoil cross sections (ref. 4). The comparison is made for a tip speed of about 310 ft/sec (94.5 m/sec), and several tip configurations of the flexible rotor are included. The results are in agreement with those of reference 1 where the flexible rotor exhibited poor efficiency while attaining high mean lift coefficients in comparison with the conventional rotor. The poor hovering efficiencies are attributed to chordwise deformations, excessive blade twist, and

inefficient planform area distribution; the attainment of the high mean lift coefficients are the result of aerodynamically induced blade camber.

Improvements in the hovering efficiency of this type of flexible rotor can be obtained by providing means of minimizing undesirable blade twist and other deformations and by providing more efficient blade planforms as pointed out in reference 1. Naturally, these improvements must not seriously compromise the requirements for a high degree of flexibility.

CONCLUSIONS

A hovering investigation of an extremely flexible lifting rotor has been conducted. The following conclusions are indicated:

1. Luffing and blade stall restrict the envelope of pitch angles and tip speeds within which this rotor can be operated. The boundaries of this envelope, particularly the luffing boundary, are dependent upon the rotor tip configuration.

2. The performance of this rotor is highly dependent upon the rotor tip speed. Deterioration in rotor hovering efficiency generally results from increasing speed. These speed effects are usually greater at the higher thrust conditions.

3. Changes in the rotor-tip configuration or operating speed affect the rotor performance through their influence on the blade twist and camber distributions. The chordwise position of the tip body center of gravity is believed to be a very important rotor parameter since it determines the blade twist axis.

4. In comparison with a conventional rotor at the same tip speed, this flexible rotor exhibits low hovering efficiencies while attaining high mean lift coefficients. The low efficiencies are attributed to chordwise blade deformations, excessive twist, and inefficient planform. The high mean lift coefficients are attributed to aerodynamically induced blade camber.

Langley Research Center,
National Aeronautics and Space Administration,
Langley Station, Hampton, Va., July 23, 1968,
721-01-00-28-23.

REFERENCES

1. Winston, Matthew M.: An Investigation of Extremely Flexible Lifting Rotors. NASA TN D-4465, 1968.
2. Pruyn, Richard R.; and Swales, Thomas G.: Development of Rotor Blades With Extreme Chordwise and Spanwise Flexibility. Proceedings Twentieth Annual National Forum, Amer. Helicopter Soc., Inc., May 1964, pp. 102-108.
3. Goldman, Robert L.: Some Observations on the Dynamic Behavior of Extremely Flexible Rotor Blades. Paper No. 60-44, Inst. Aero. Sci., Jan. 1960.
4. Carpenter, Paul J.: Lift and Profile-Drag Characteristics of an NACA 0012 Airfoil Section as Derived From Measured Helicopter-Rotor Hovering Performance. NACA TN 4357, 1958.
5. Mechtly, E. A.: The International System of Units - Physical Constants and Conversion Factors. NASA SP-7012, 1964.

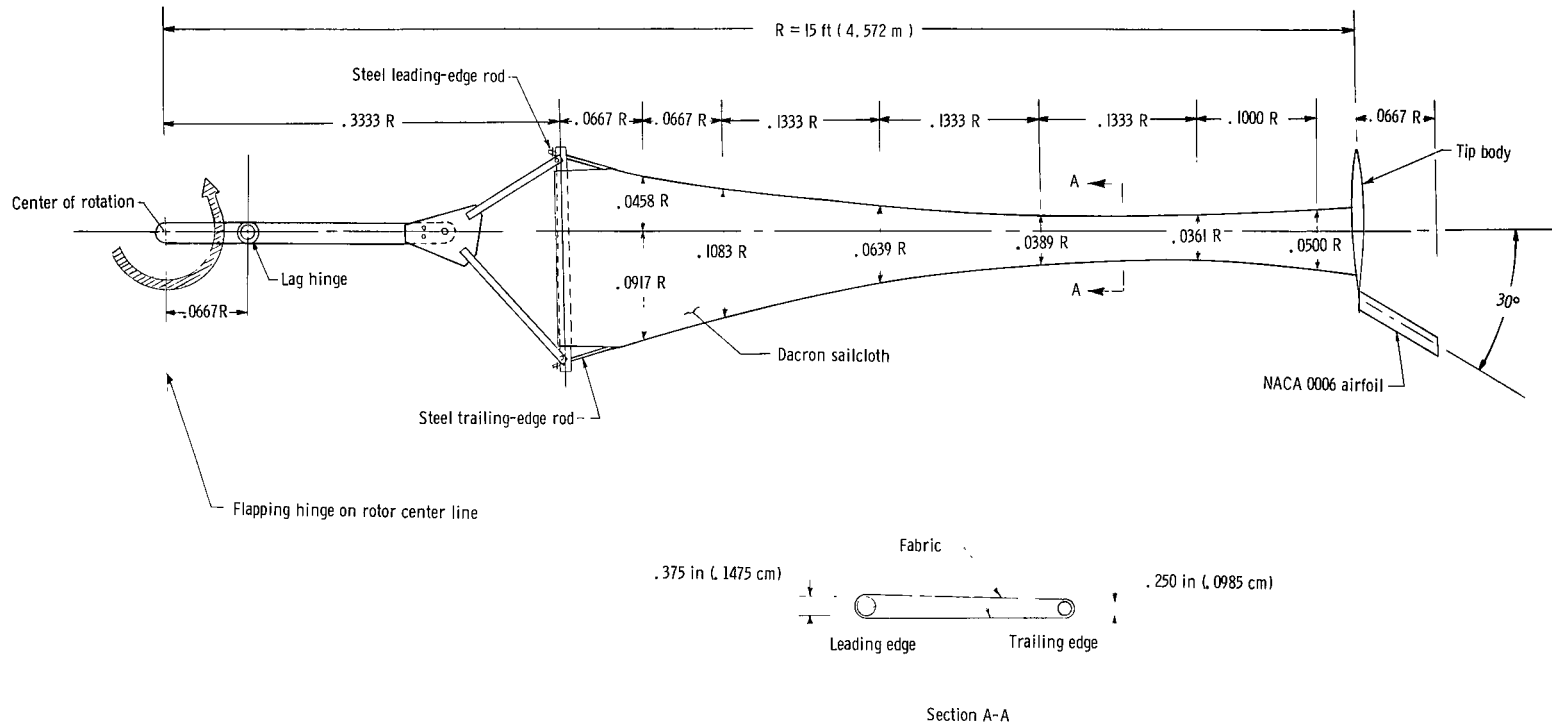


Figure 1.- Principal dimensions of experimental flexible rotor blades.



Figure 2.- Experimental rotor mounted on Langley helicopter test tower.

L-68-811

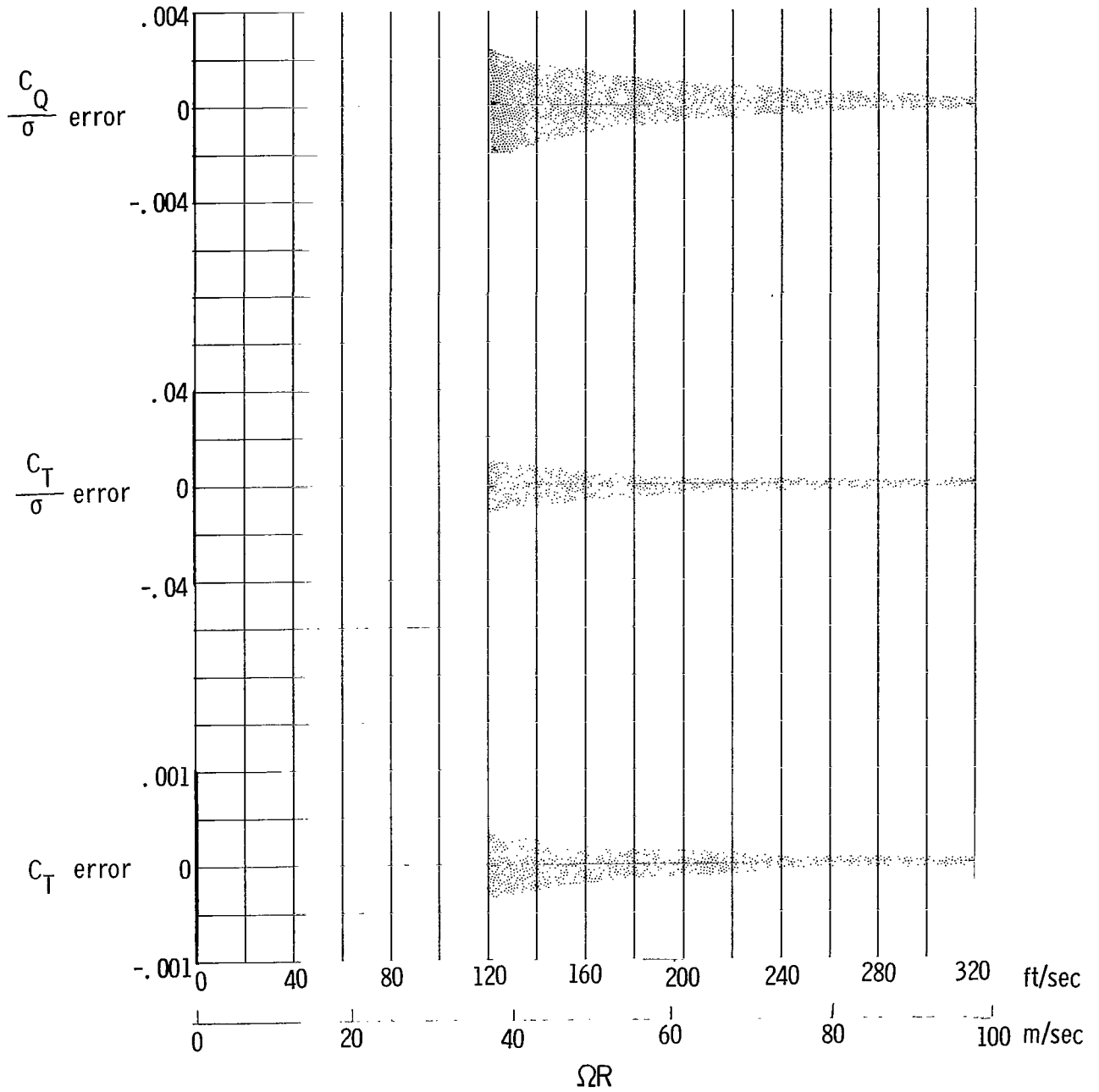


Figure 3.- Probable error in measurements of thrust and torque coefficients as a function of tip speed.

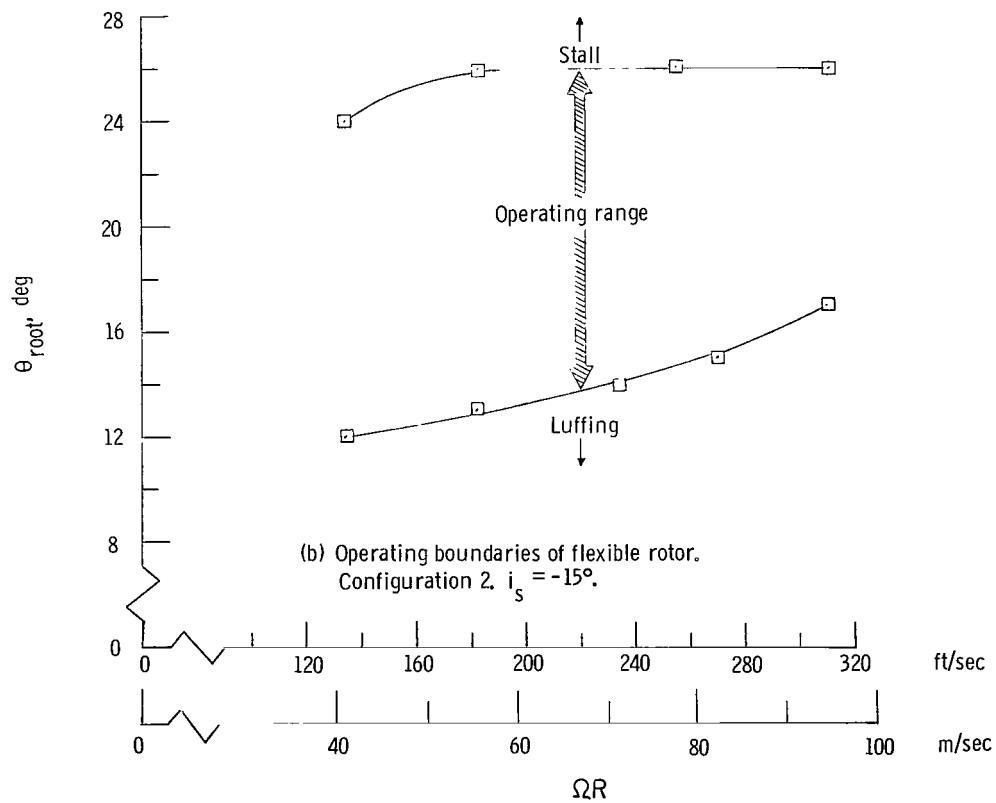
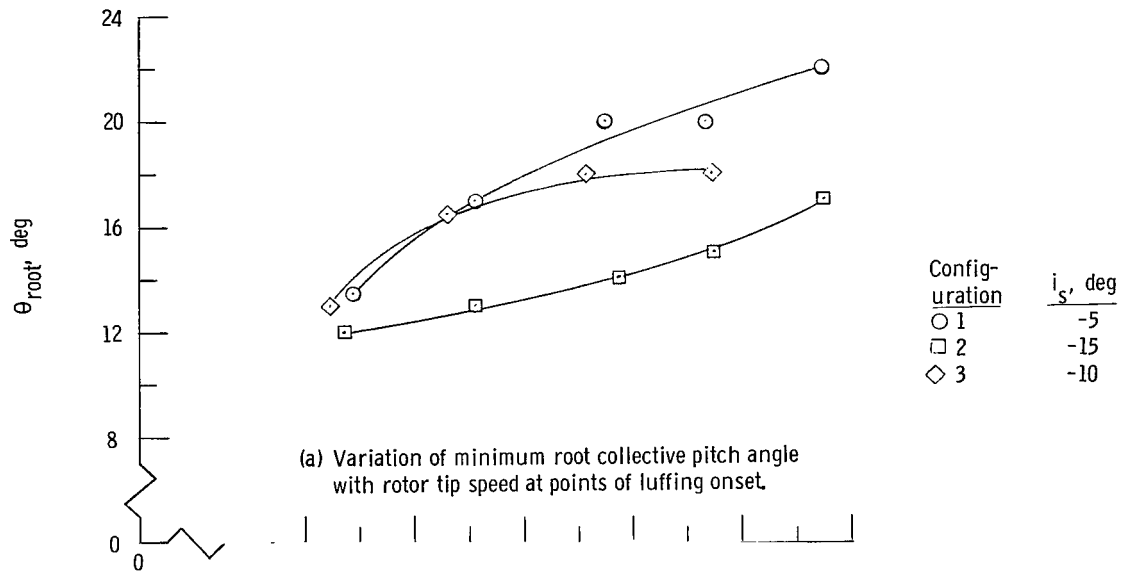
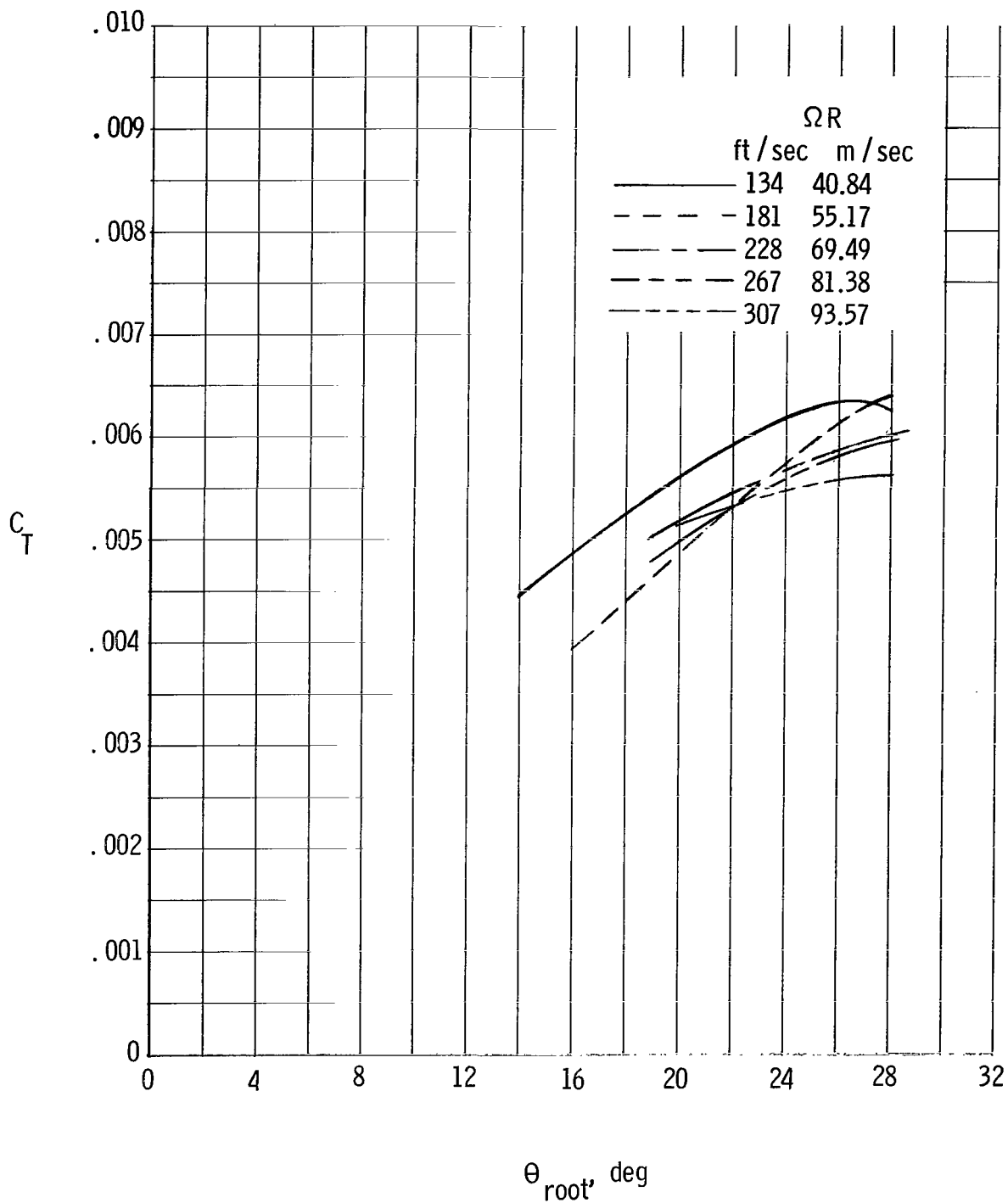
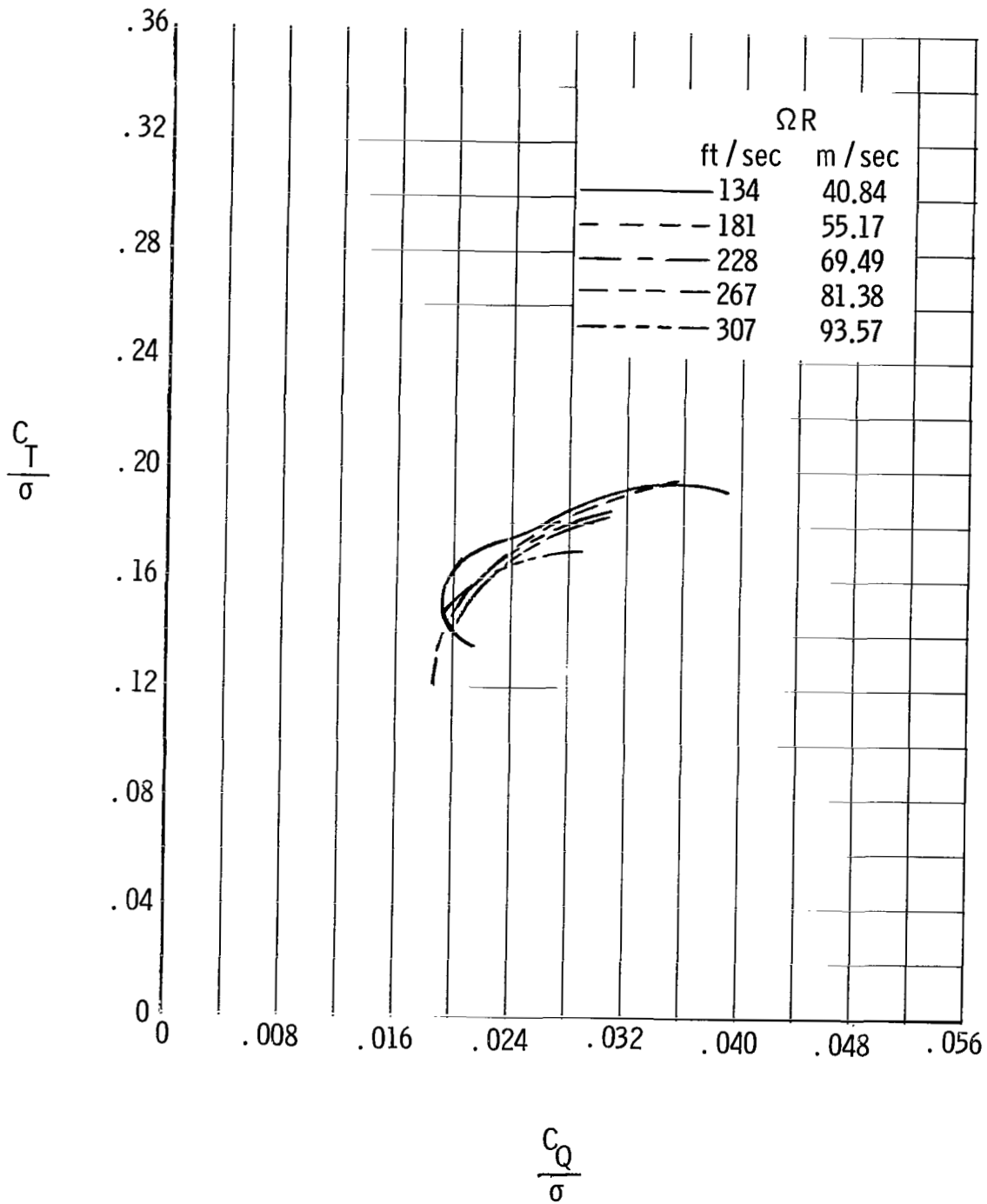


Figure 4.- Flexible-rotor luffing characteristics.



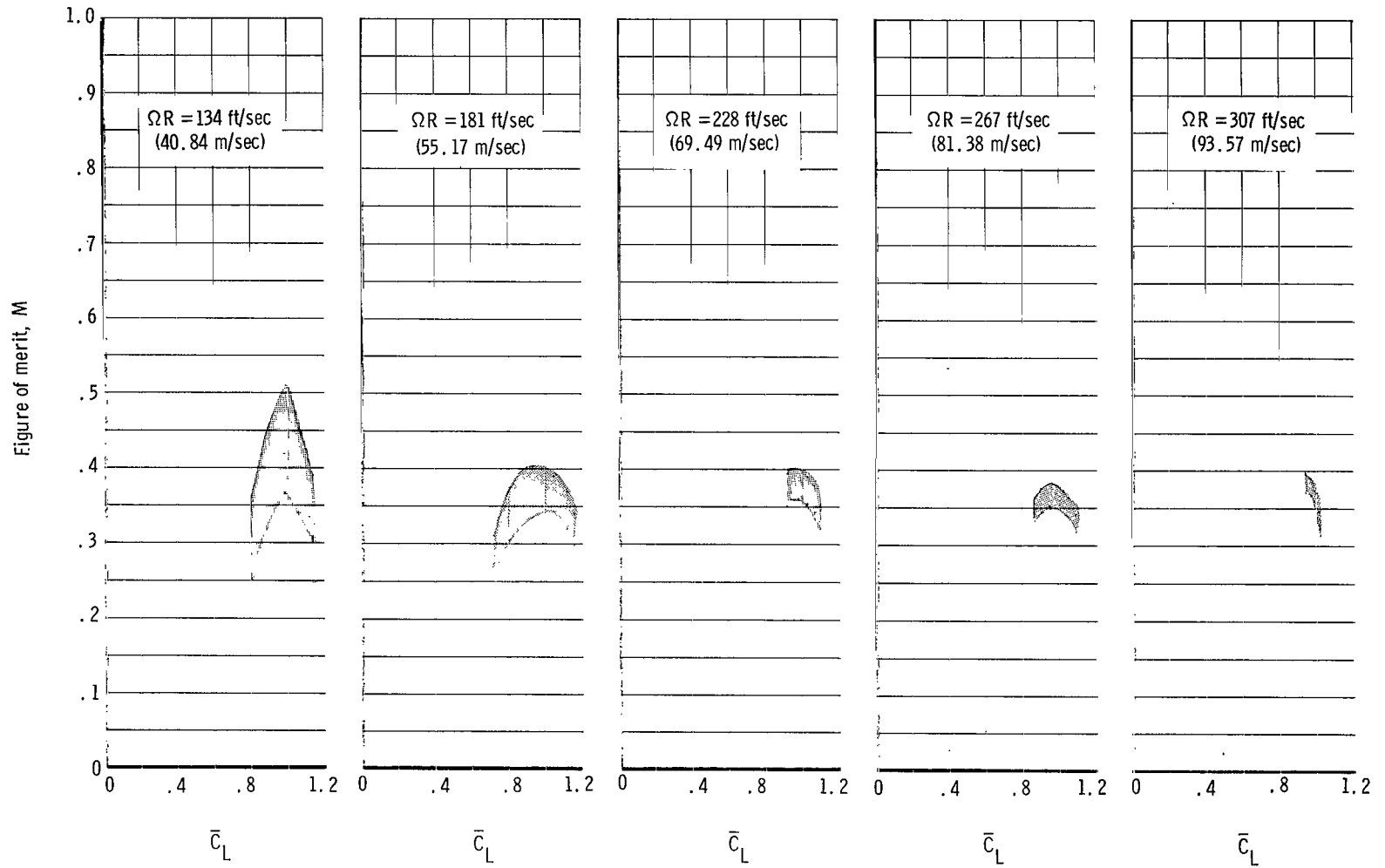
(a) Variation of thrust coefficient with root pitch angle.

Figure 5.- Hovering characteristics of configuration 1. $i_s = -5^\circ$.



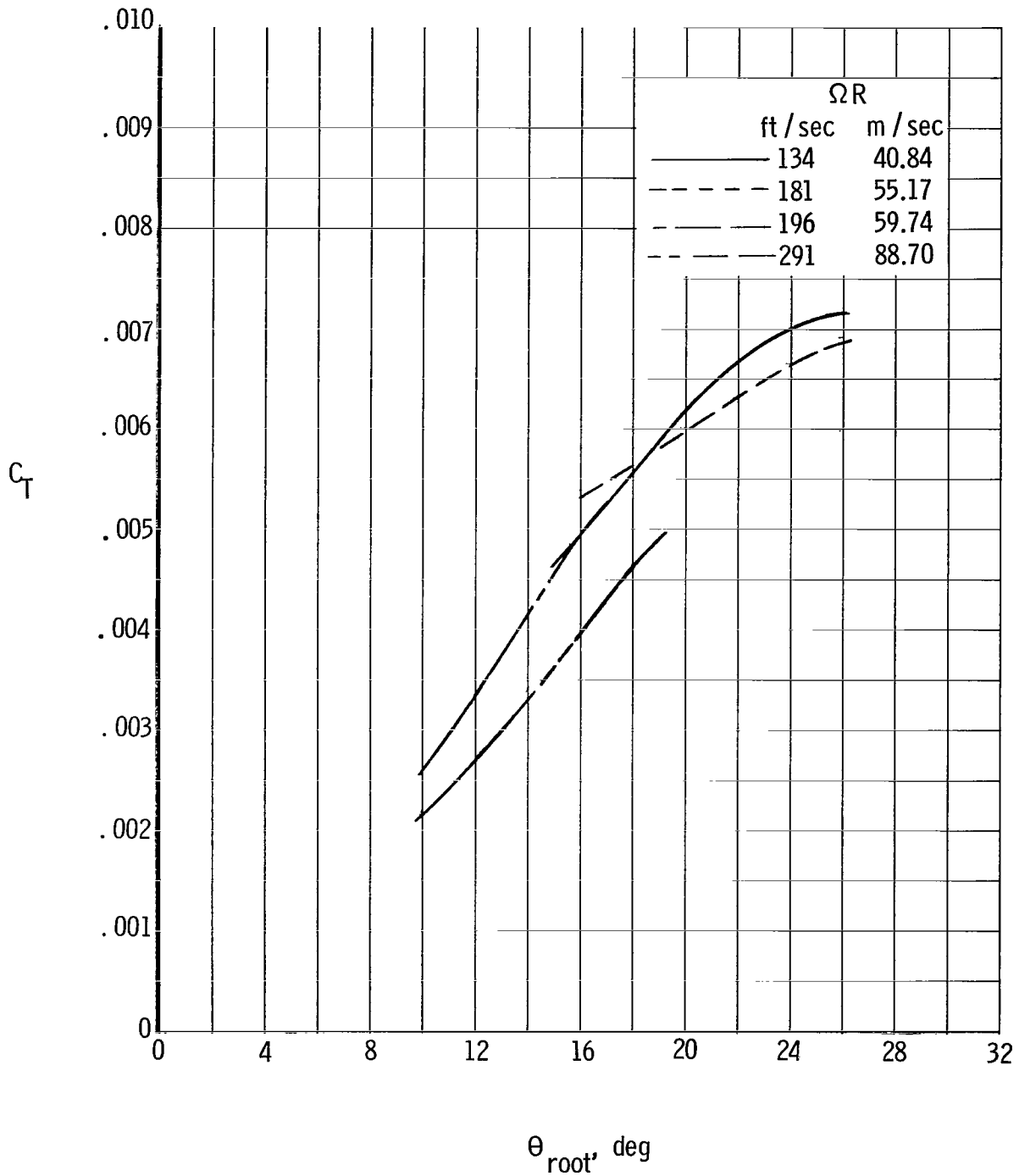
(b) Variation of thrust-coefficient—solidity ratio with torque-coefficient—solidity ratio.

Figure 5.- Continued.



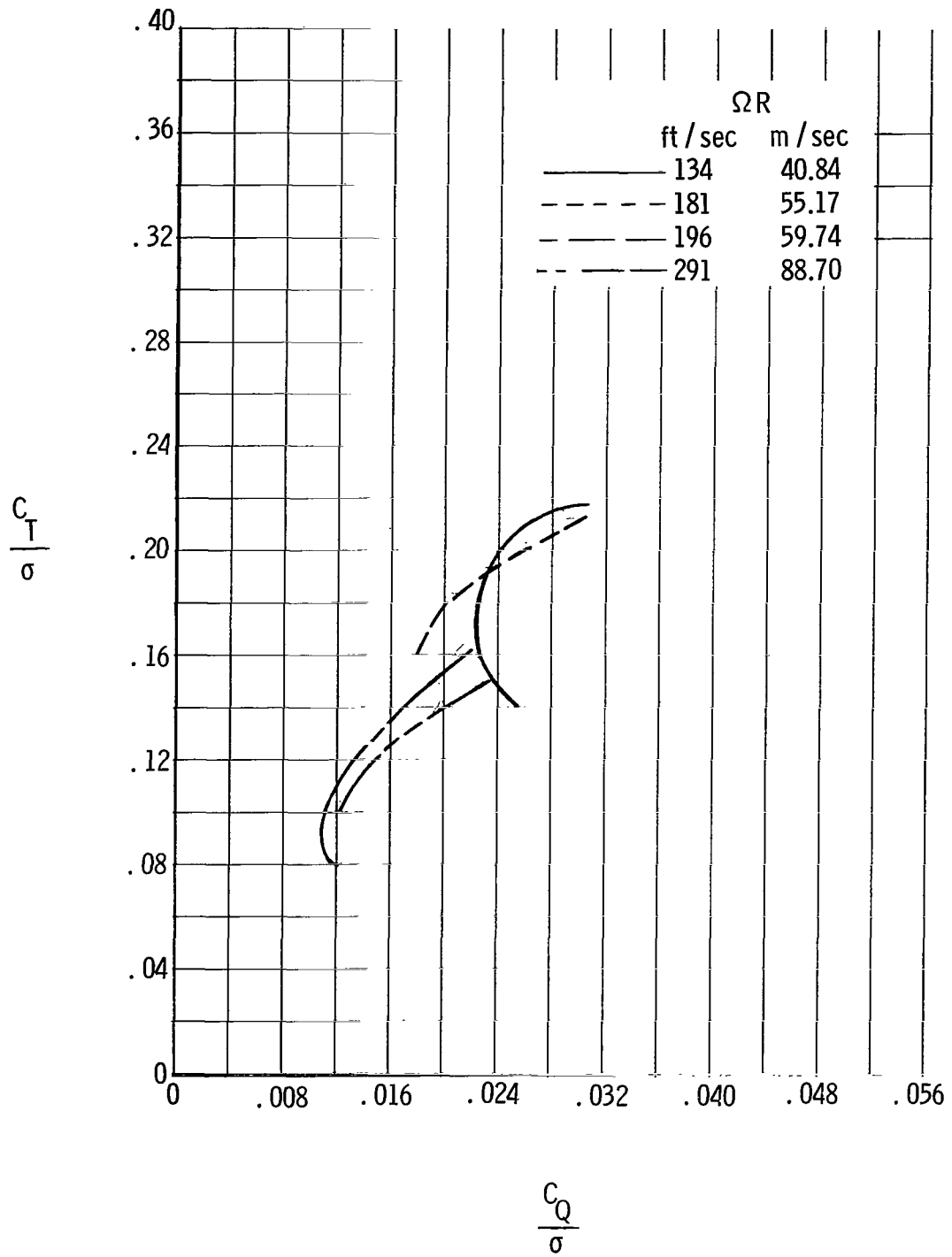
(c) Variation of rotor figure of merit with mean lift coefficient.

Figure 5.- Concluded.



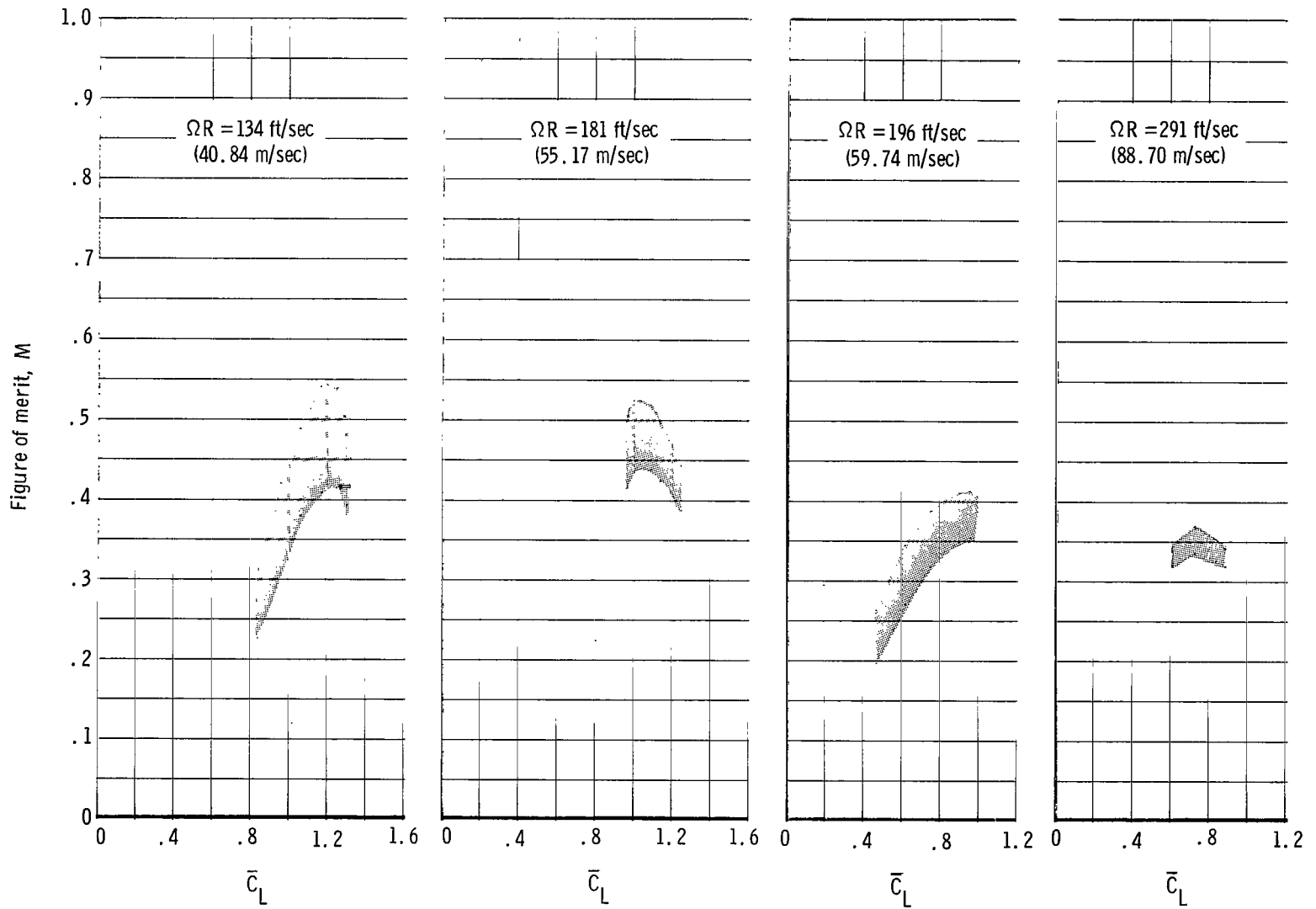
(a) Variation of thrust coefficient with root pitch angle.

Figure 6.- Hovering characteristics of configuration 1. $i_s = -10^\circ$.



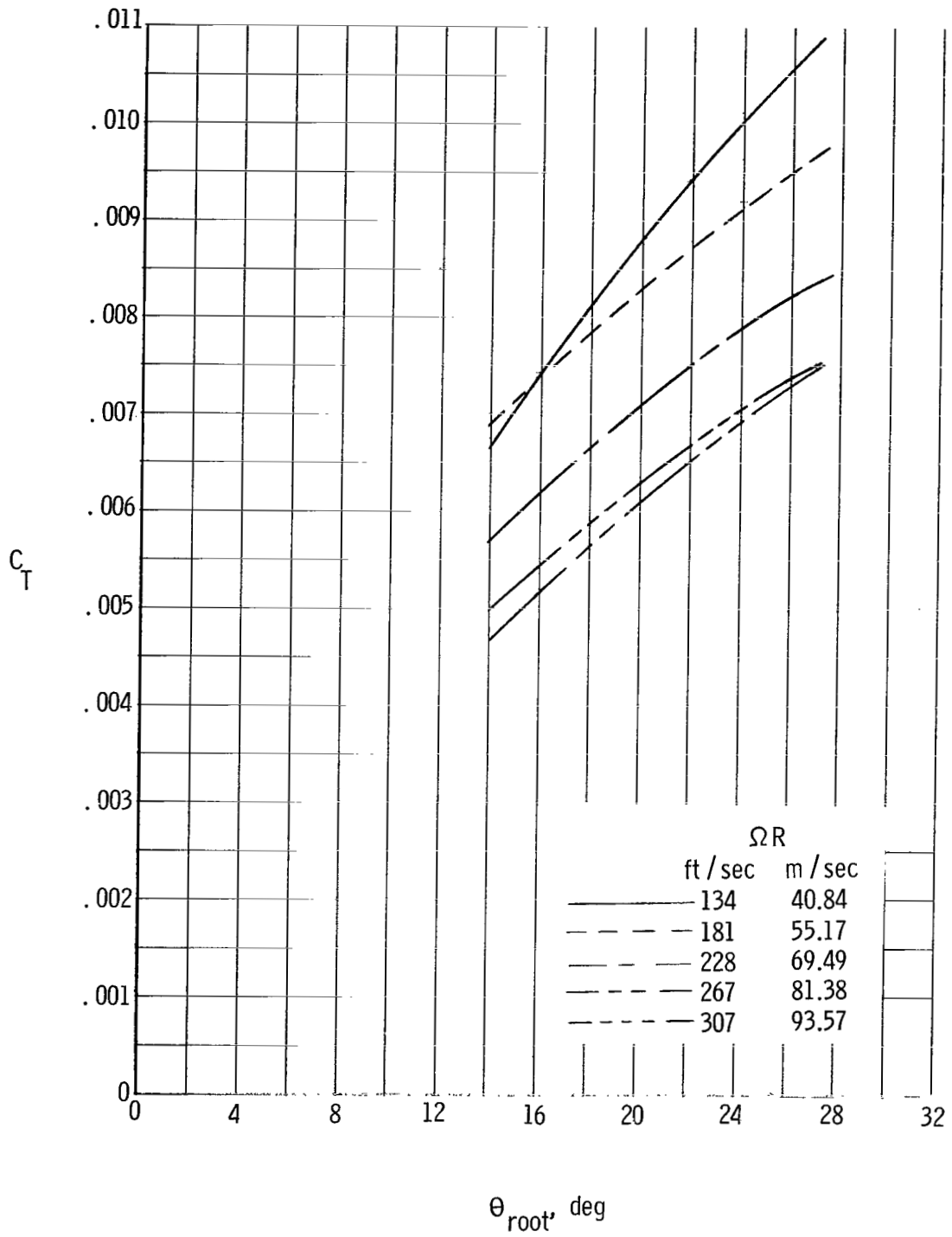
(b) Variation of thrust-coefficient—solidity ratio with torque-coefficient—solidity ratio.

Figure 6.- Continued.



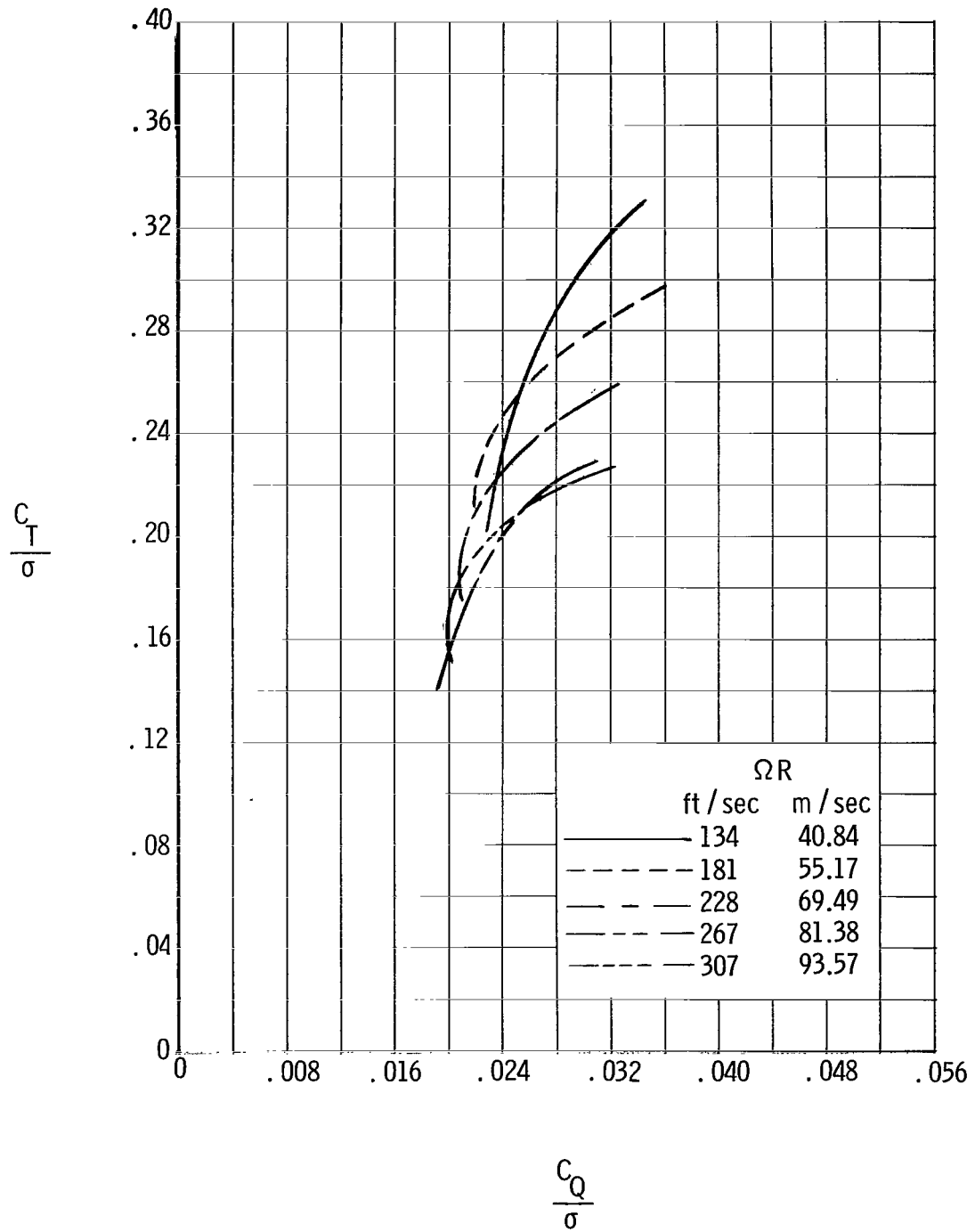
(c) Variation of rotor figure of merit with mean lift coefficient.

Figure 6.- Concluded.



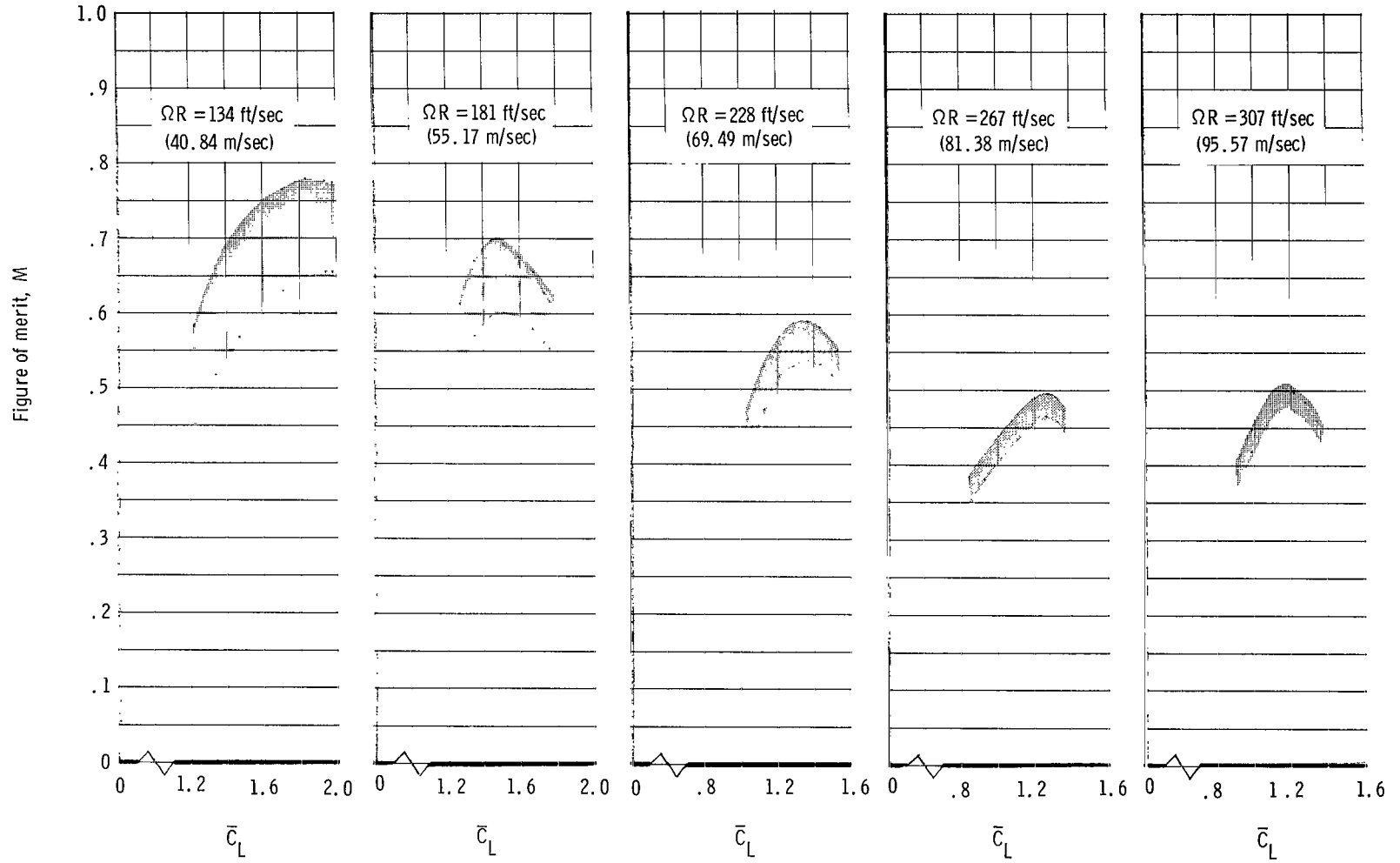
(a) Variation of thrust coefficient with root pitch angle.

Figure 7.- Hovering characteristics of configuration 1. $i_s = -15^\circ$.



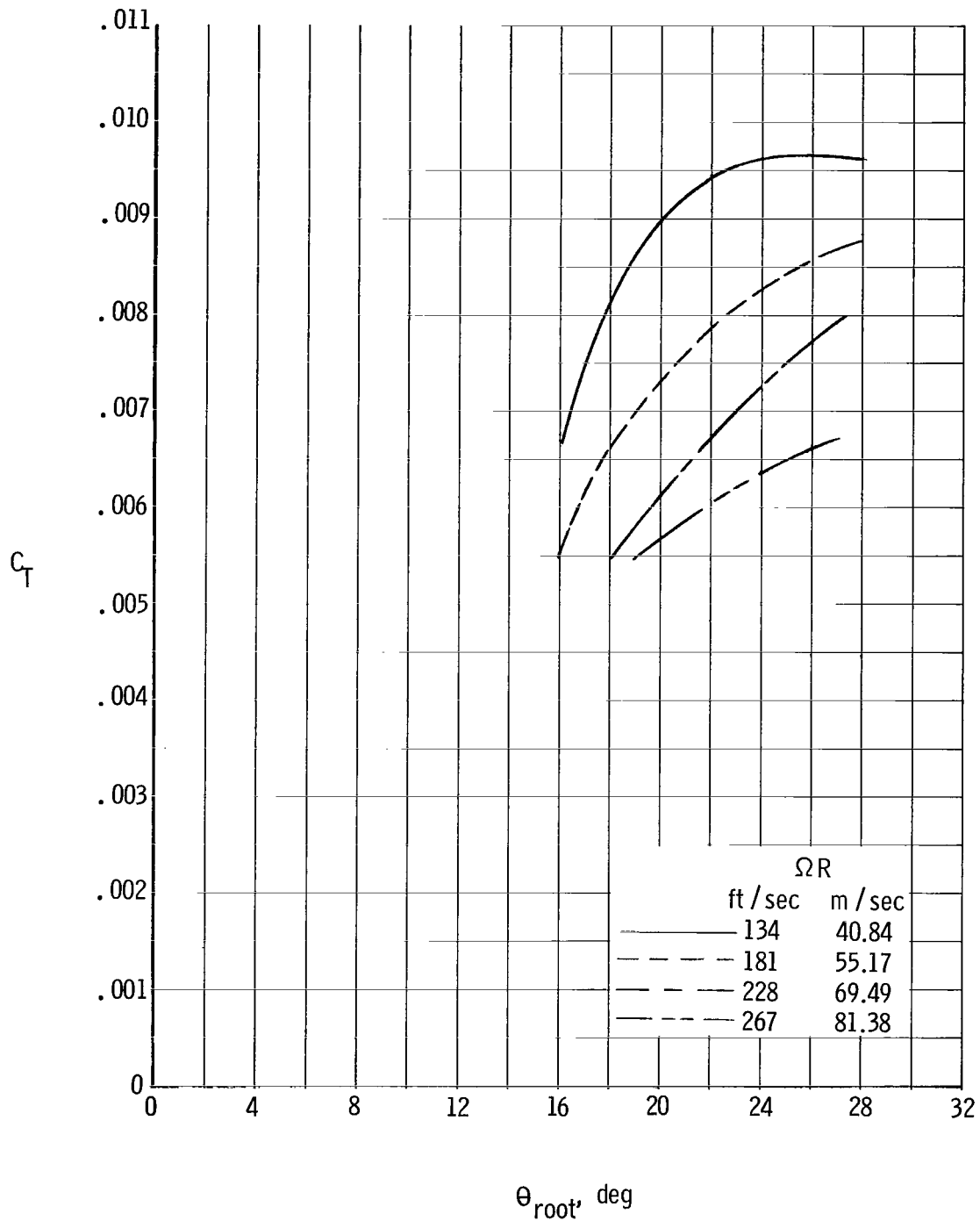
(b) Variation of thrust-coefficient—solidity ratio with torque-coefficient—solidity ratio.

Figure 7.- Continued.



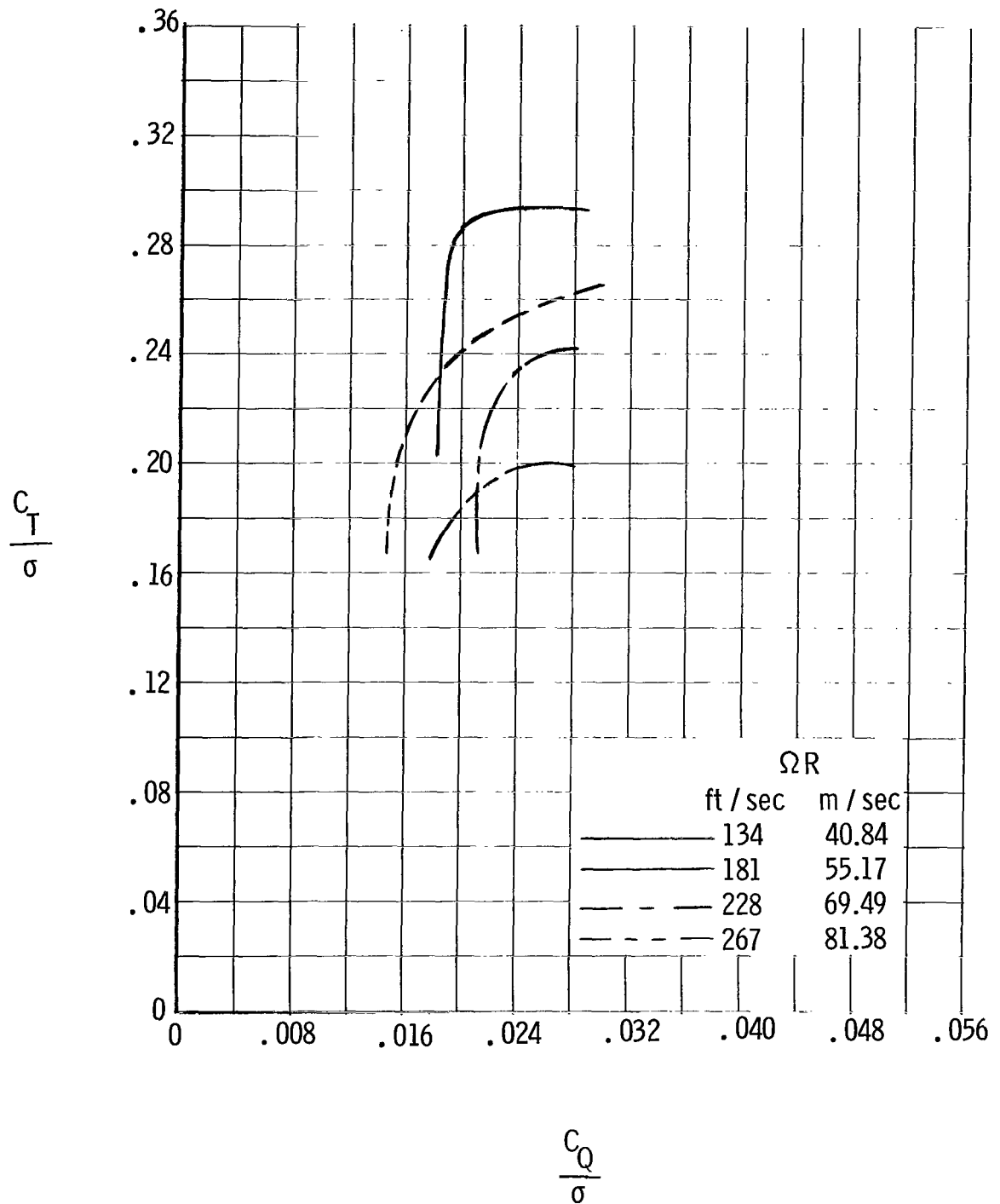
(c) Variation of rotor figure of merit with mean lift coefficient.

Figure 7.- Concluded.



(a) Variation of thrust coefficient with root pitch angle.

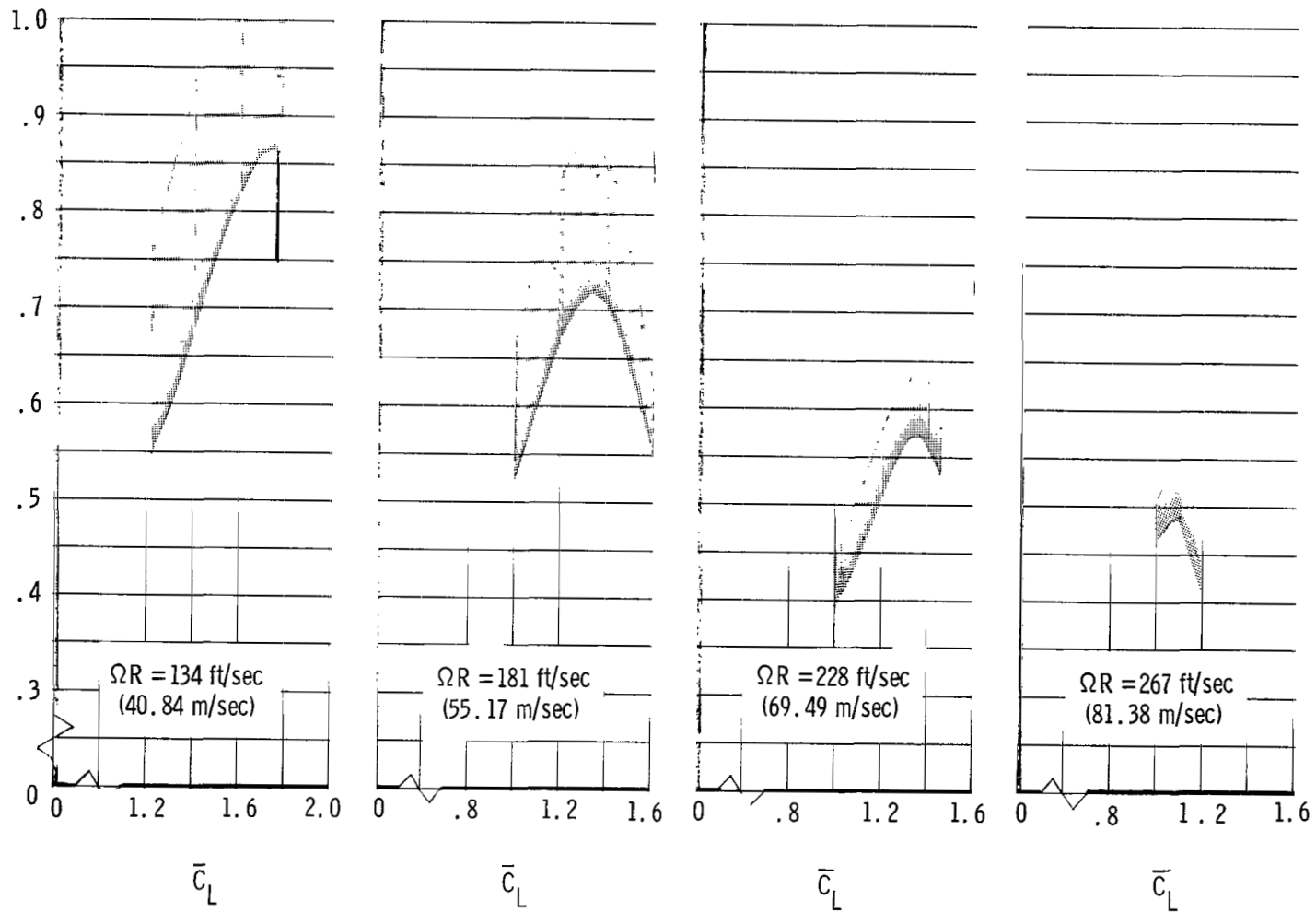
Figure 8.- Hovering characteristics of configuration 2. $i_s = -5^\circ$.



(b) Variation of thrust-coefficient—solidity ratio with torque-coefficient—solidity ratio.

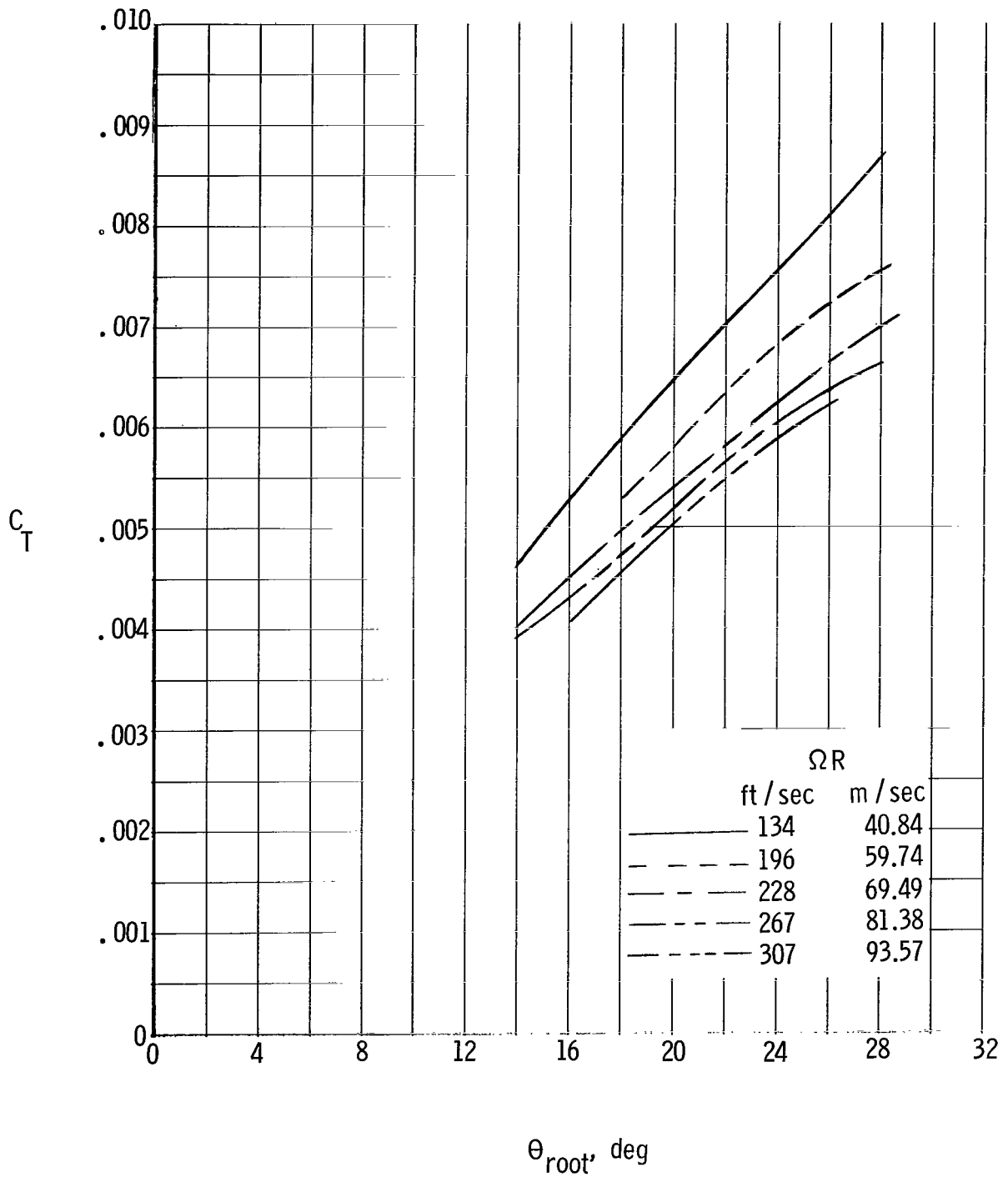
Figure 8.- Continued.

Figure of merit, M



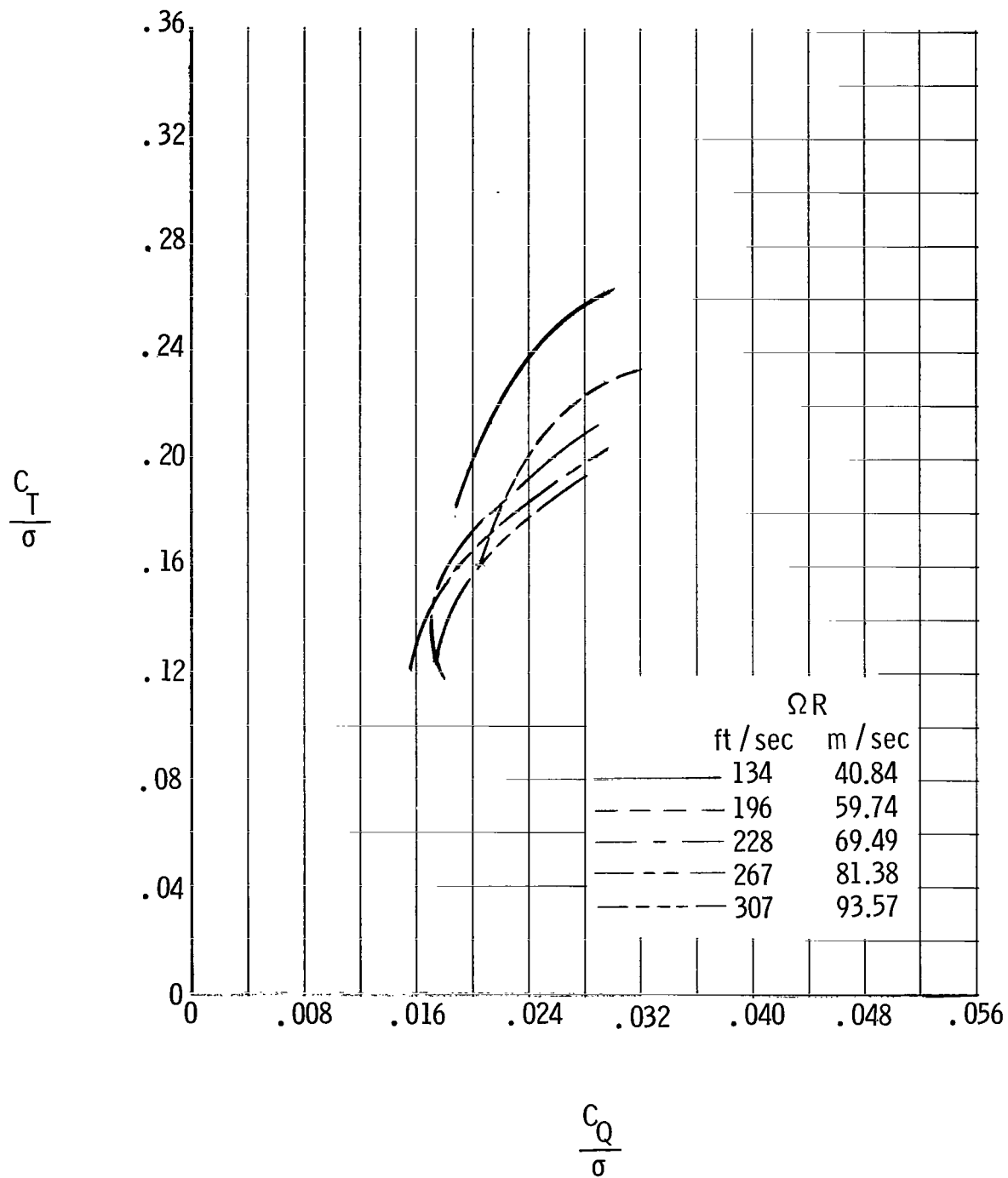
(c) Variation of rotor figure of merit with mean lift coefficient.

Figure 8.- Concluded.



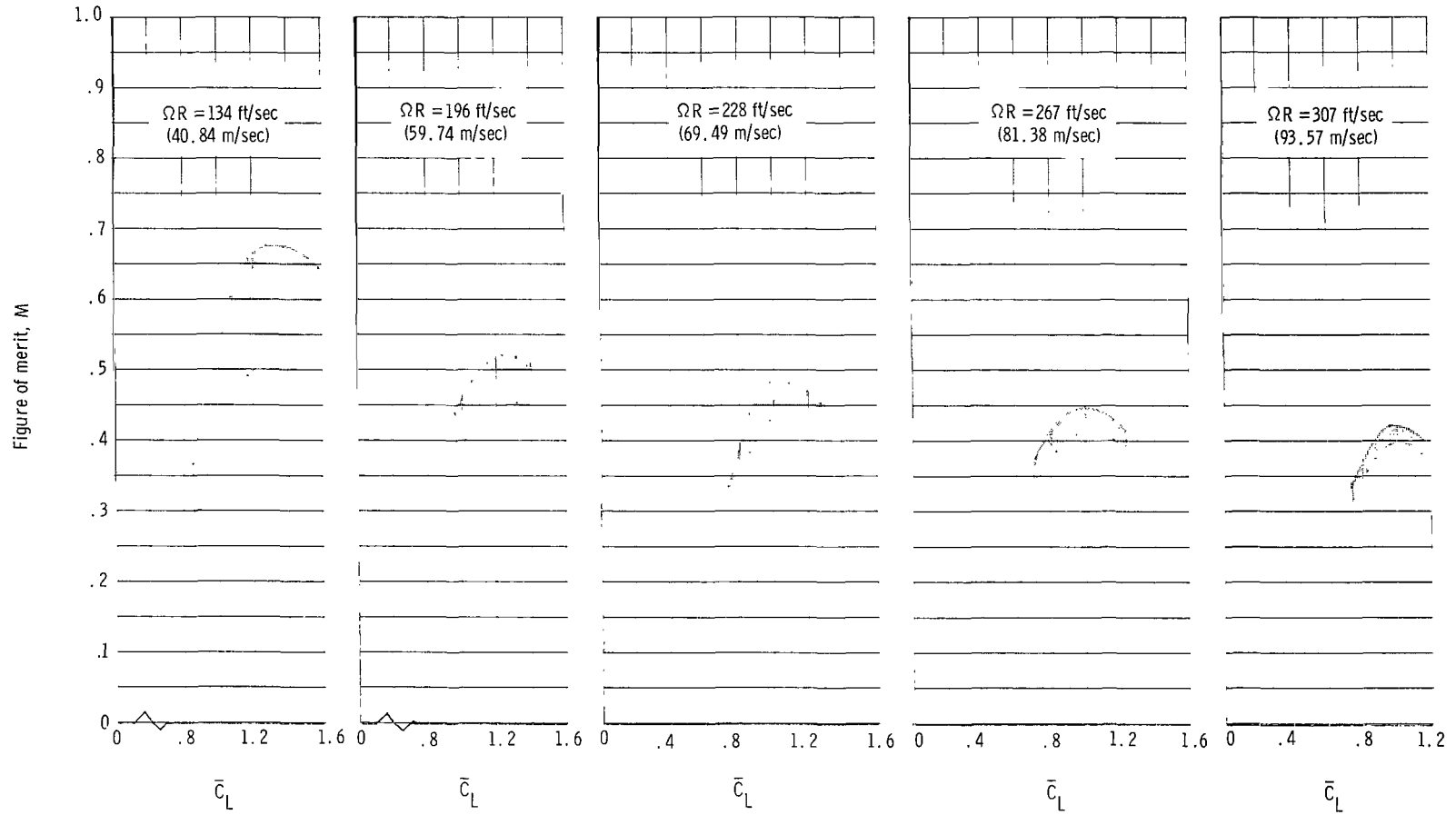
(a) Variation of thrust coefficient with root pitch angle.

Figure 9.- Hovering characteristics of configuration 2. $i_s = -10^\circ$.



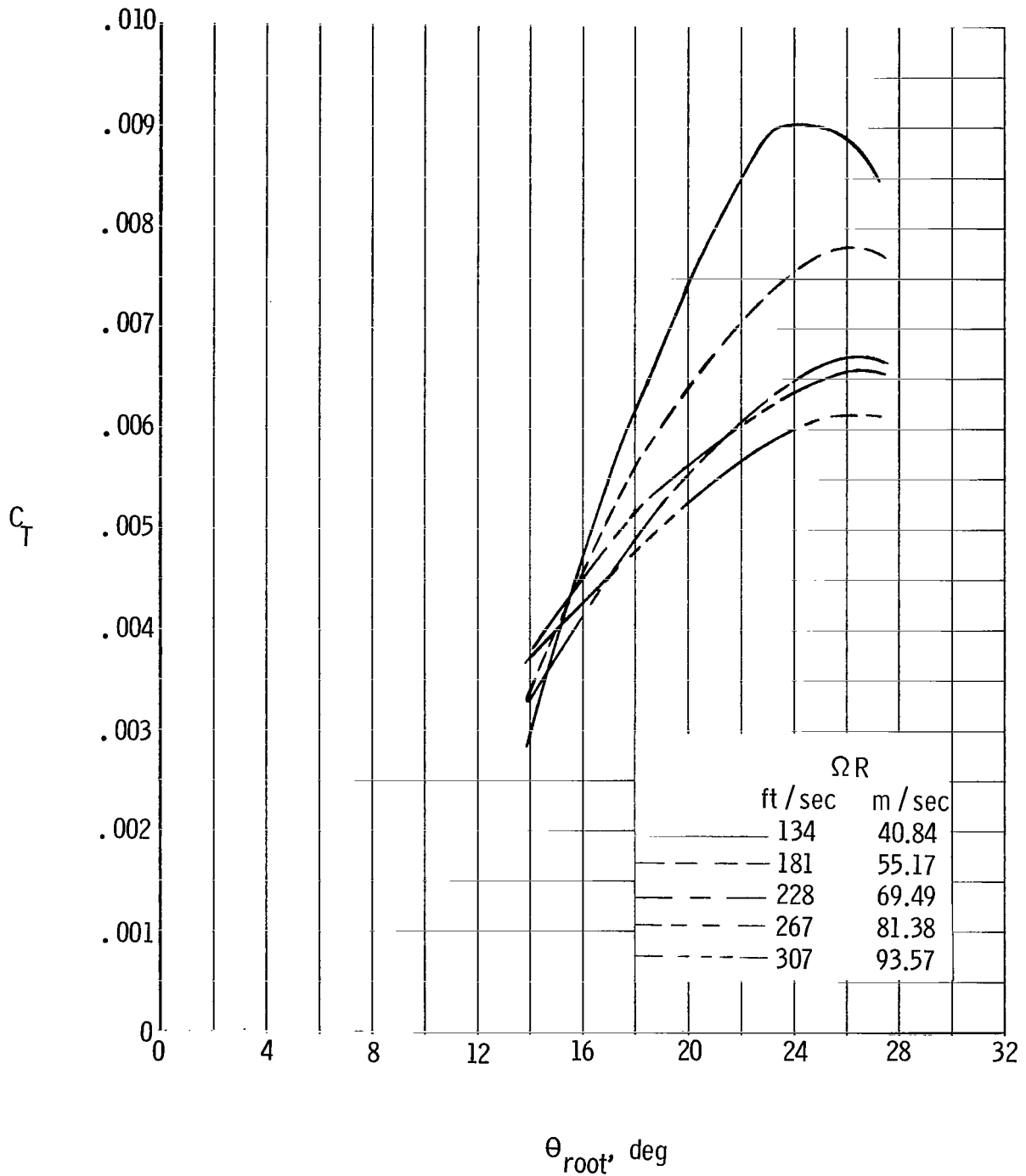
(b) Variation of thrust-coefficient—solidity ratio with torque-coefficient—solidity ratio.

Figure 9.- Continued.



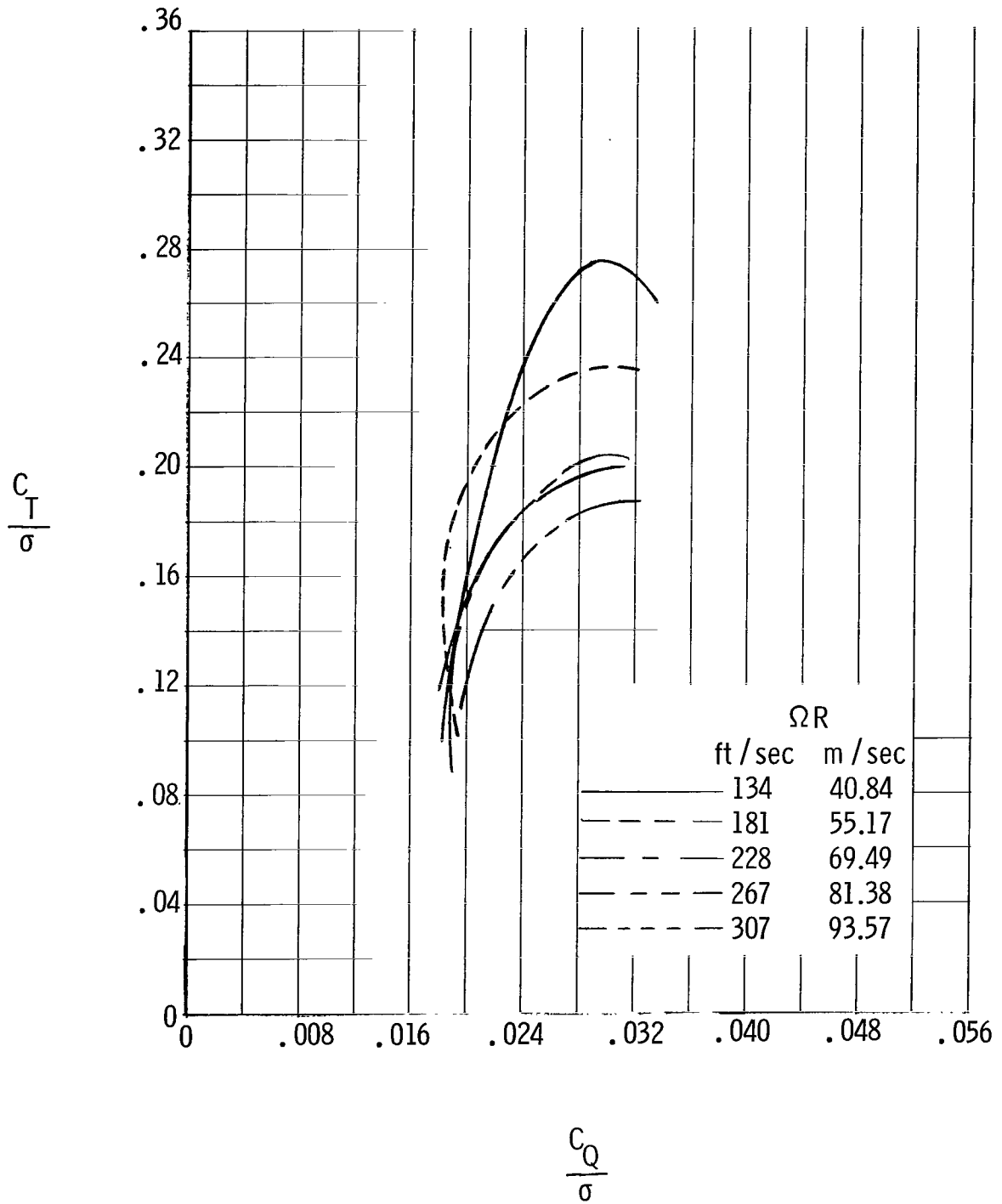
(c) Variation of rotor figure of merit with mean lift coefficient.

Figure 9.- Concluded.



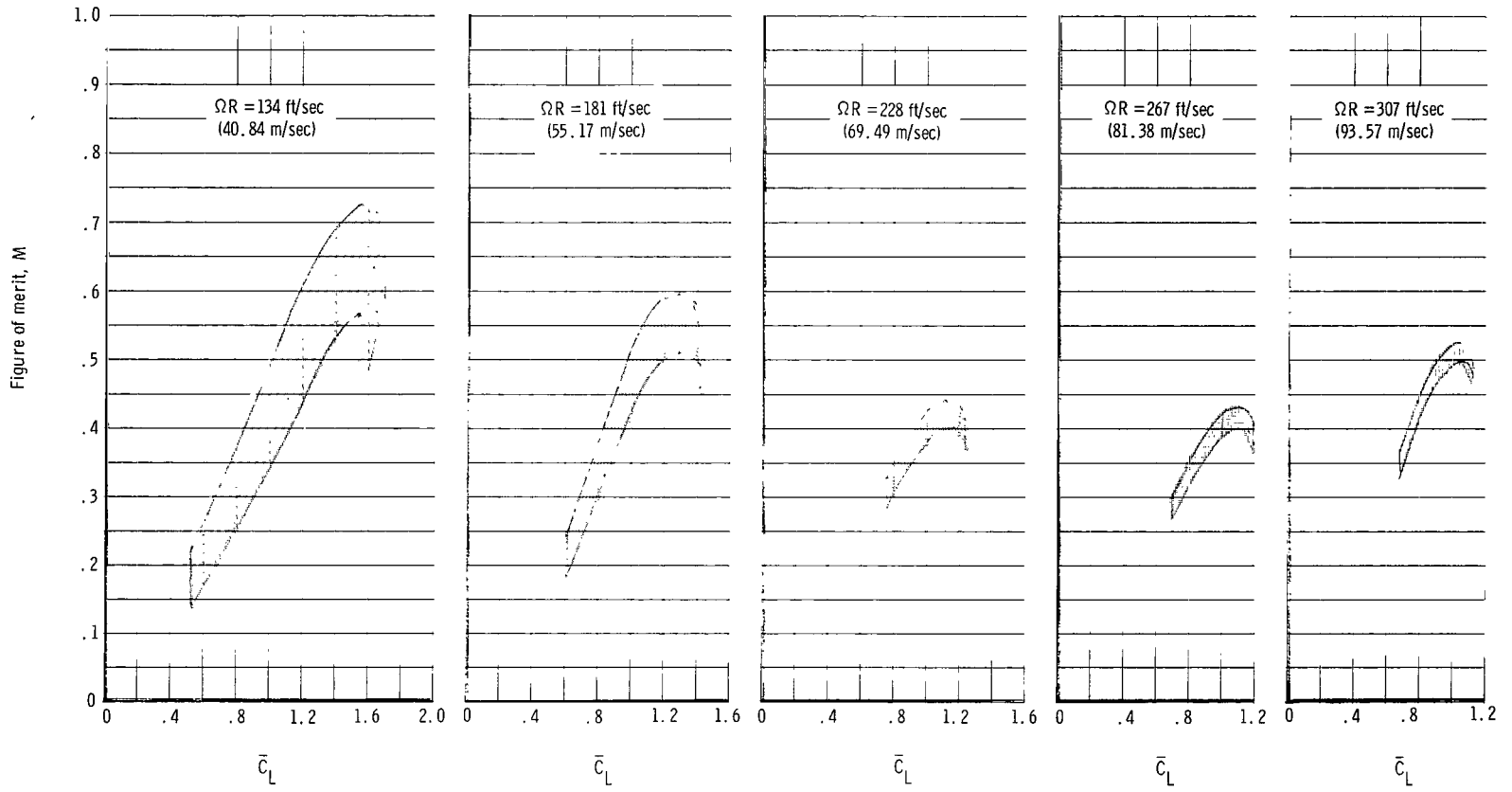
(a) Variation of thrust coefficient with root pitch angle.

Figure 10.- Hovering characteristics of configuration 2. $i_s = -15^\circ$.



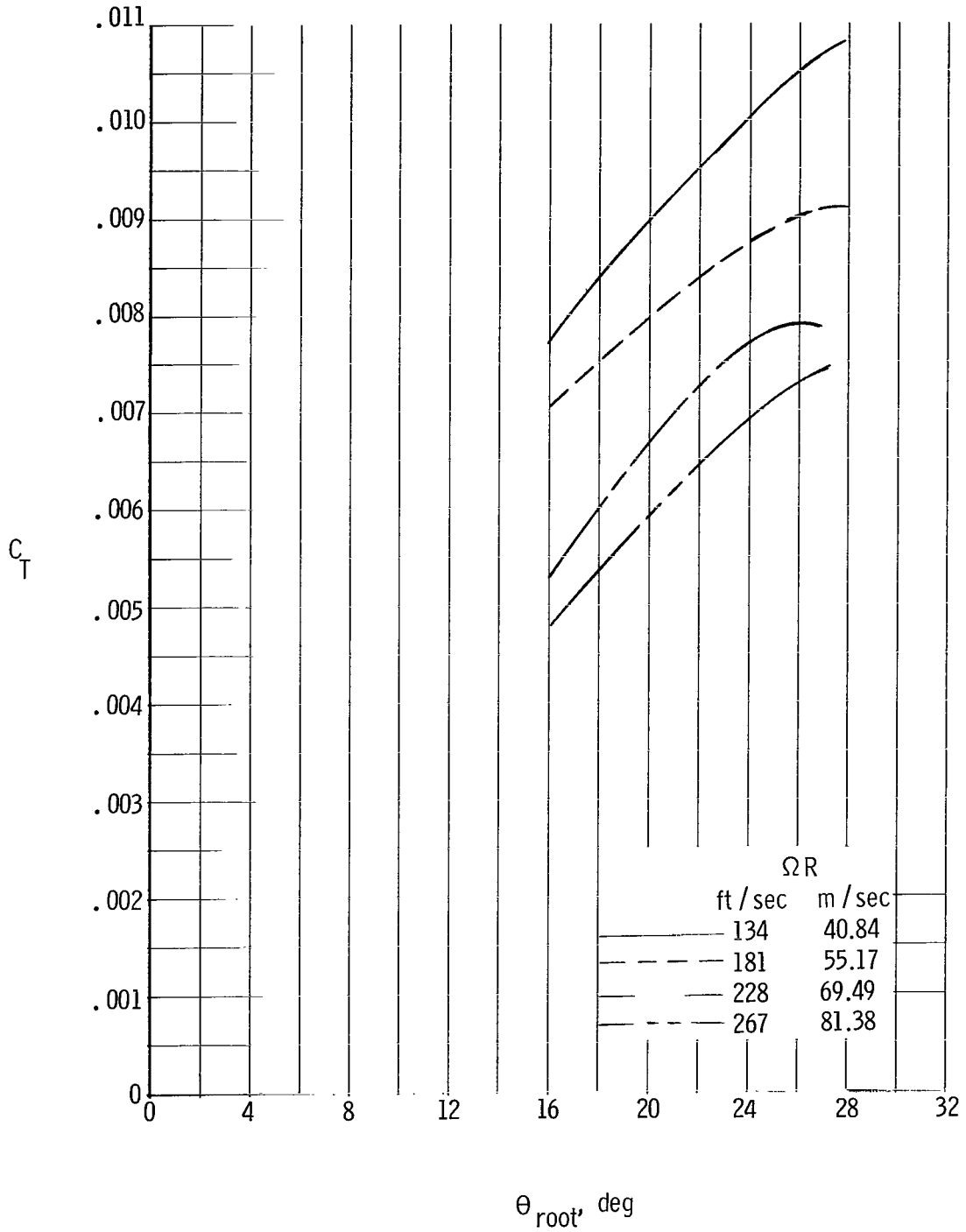
(b) Variation of thrust-coefficient—solidity ratio with torque-coefficient—solidity ratio.

Figure 10.- Continued.



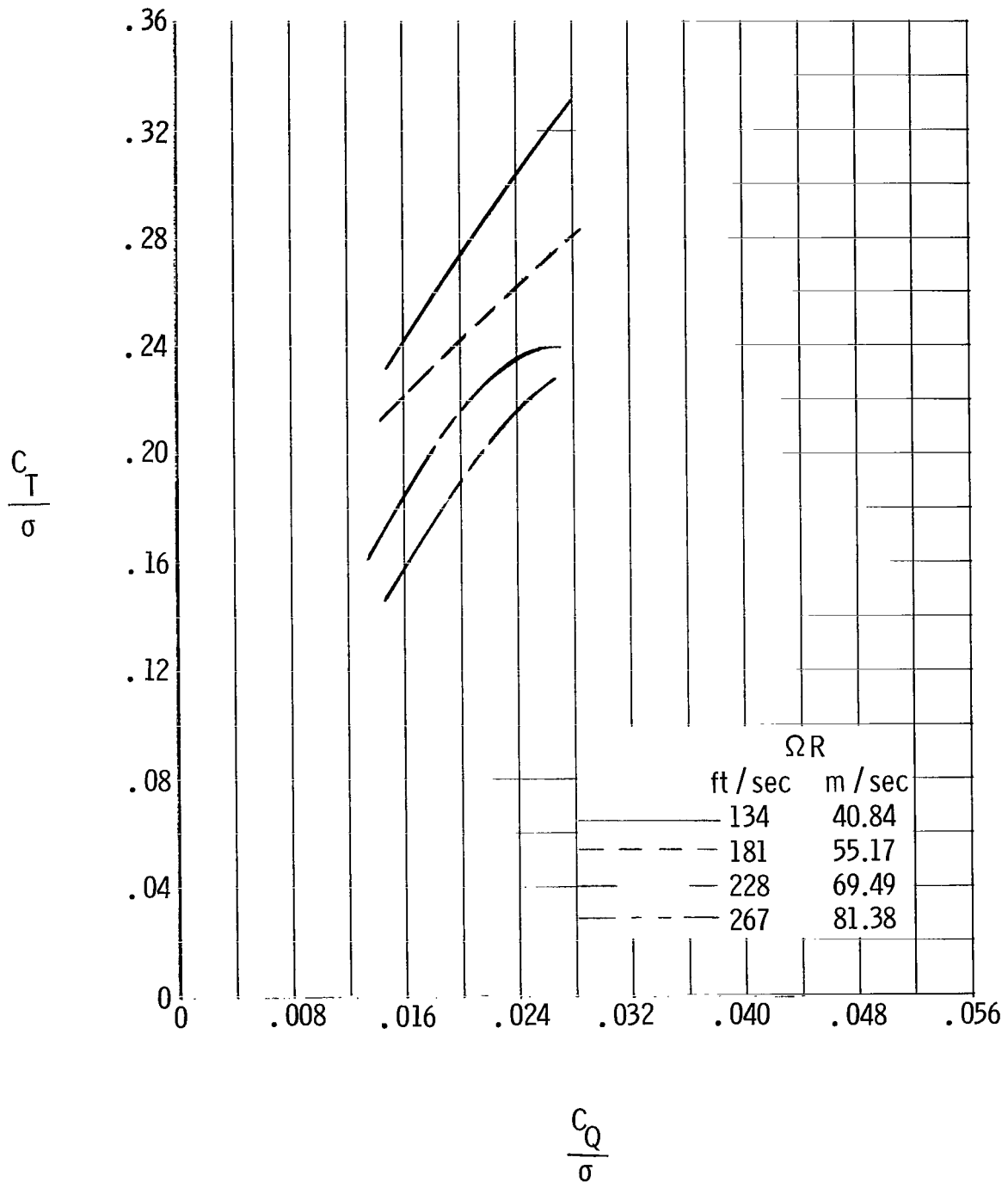
(c) Variation of rotor figure of merit with mean lift coefficient.

Figure 10.- Concluded.



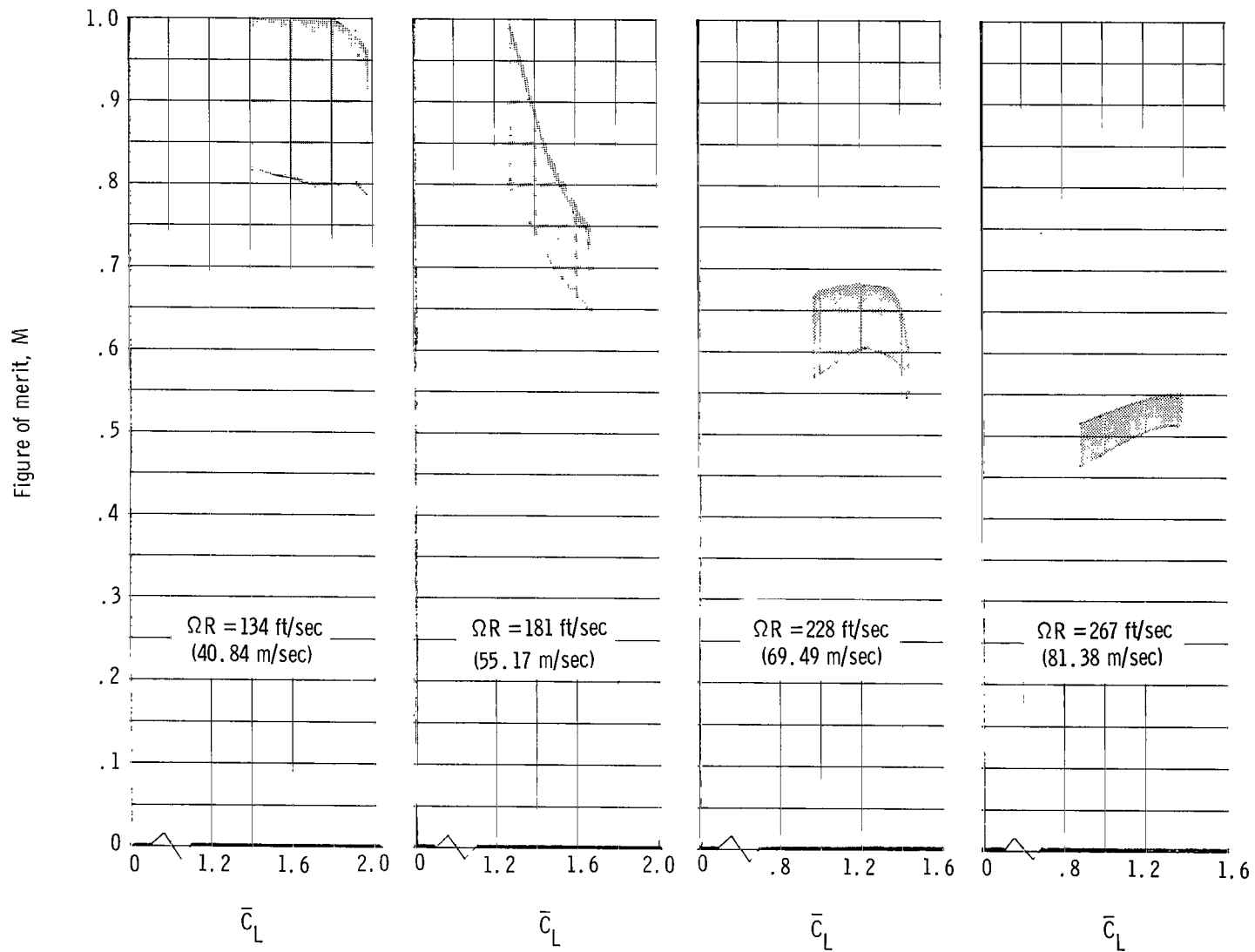
(a) Variation of thrust coefficient with root pitch angle.

Figure 11.- Hovering characteristics of configuration 3. $i_s = -10^\circ$.



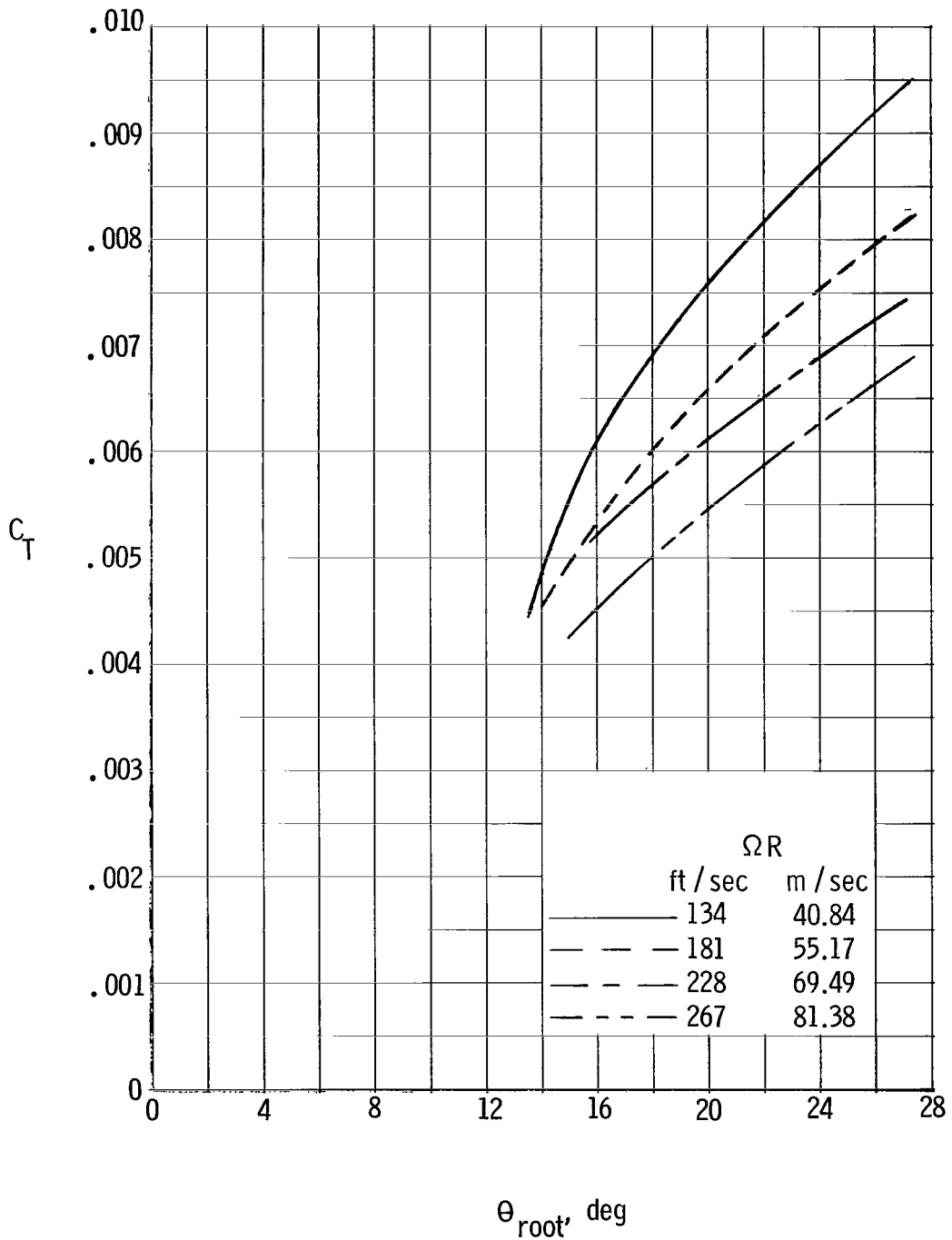
(b) Variation of thrust-coefficient—solidity ratio with torque-coefficient—solidity ratio.

Figure 11.- Continued.



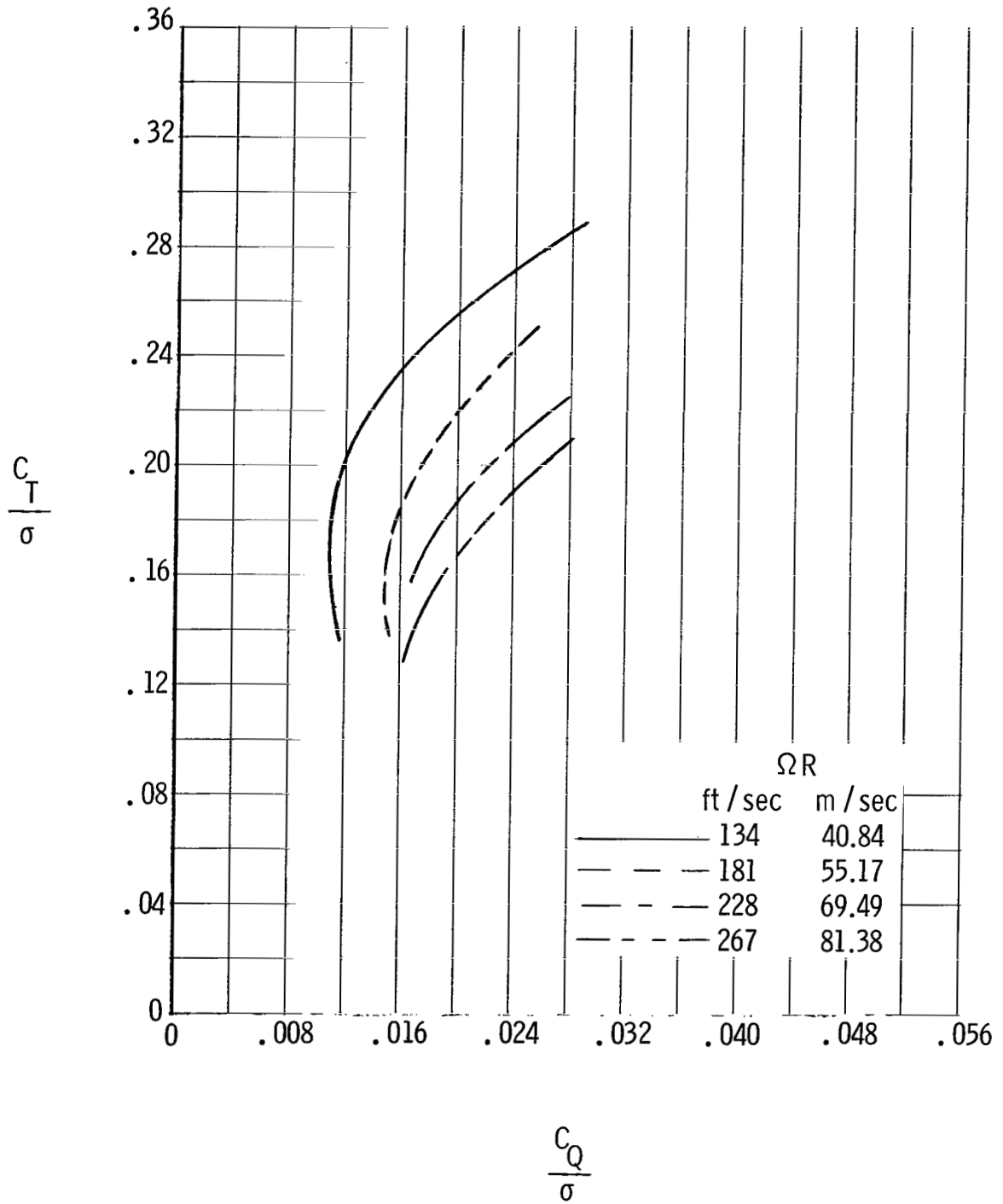
(c) Variation of rotor figure of merit with mean lift coefficient.

Figure 11.- Concluded.



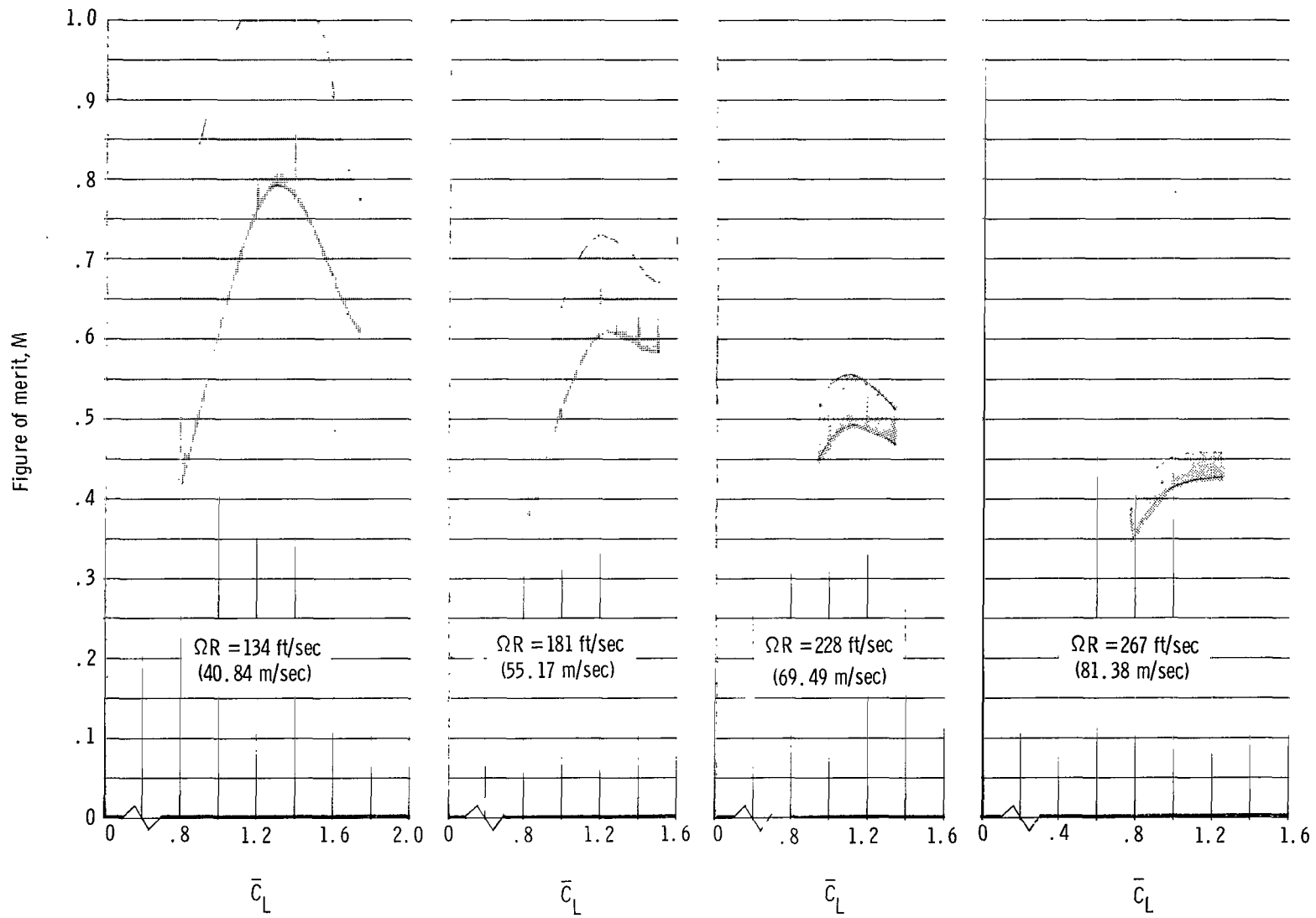
(a) Variation of thrust coefficient with root pitch angle.

Figure 12.- Hovering characteristics of configuration 3. $i_s = -15^\circ$.



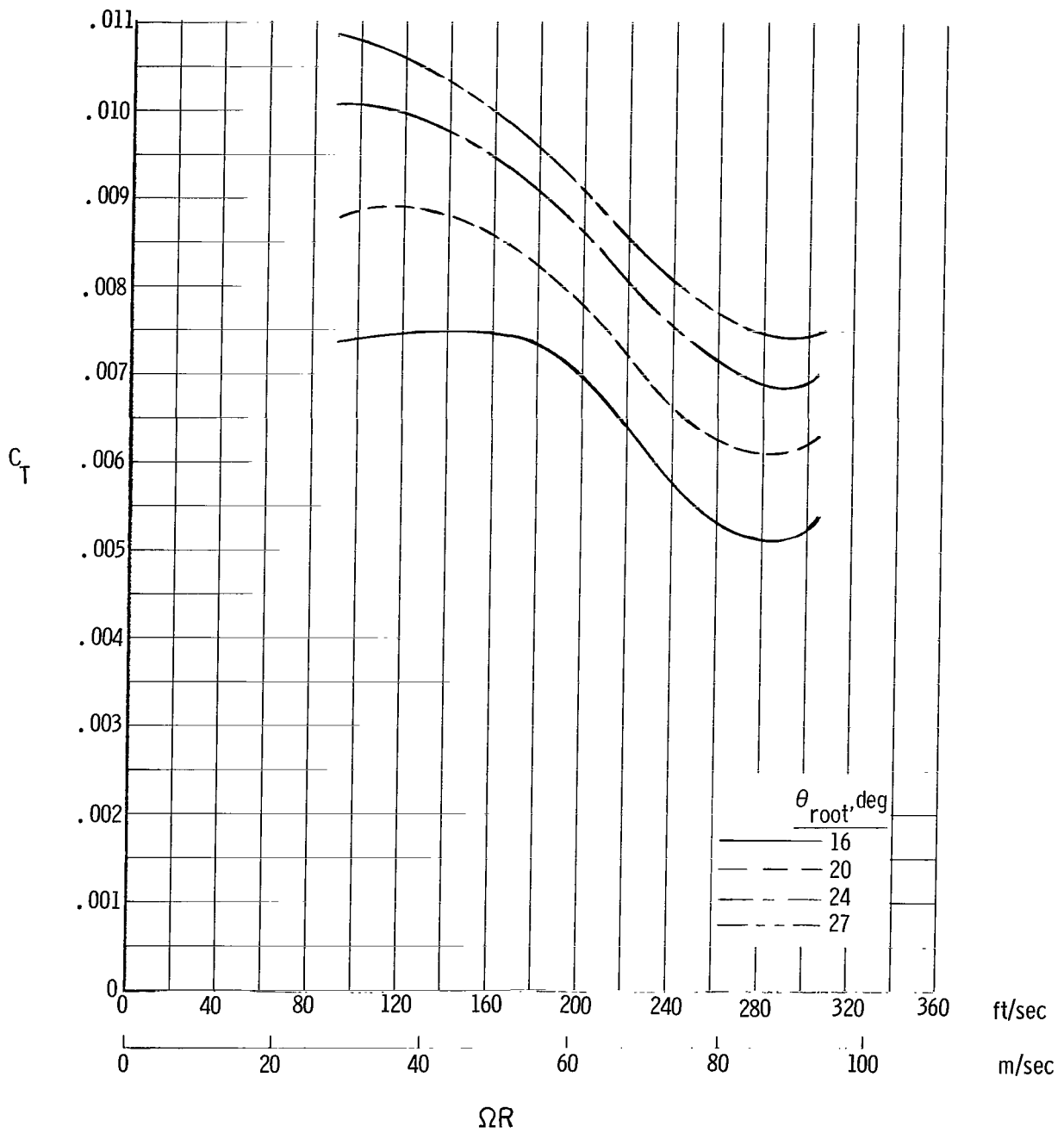
(b) Variation of thrust-coefficient—solidity ratio with torque-coefficient—solidity ratio.

Figure 12.- Continued.



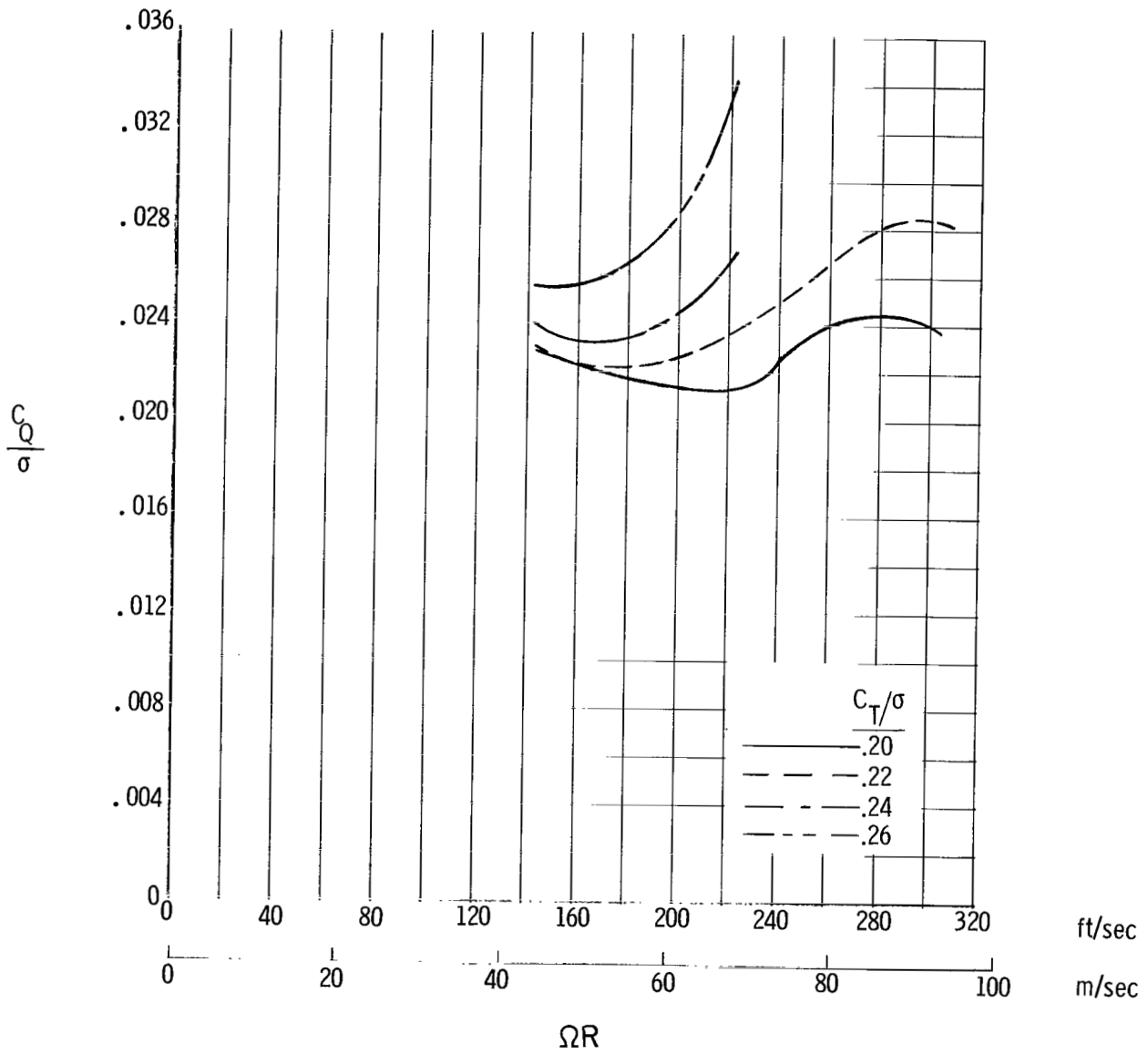
(c) Variation of rotor figure of merit with mean lift coefficient.

Figure 12.- Concluded.



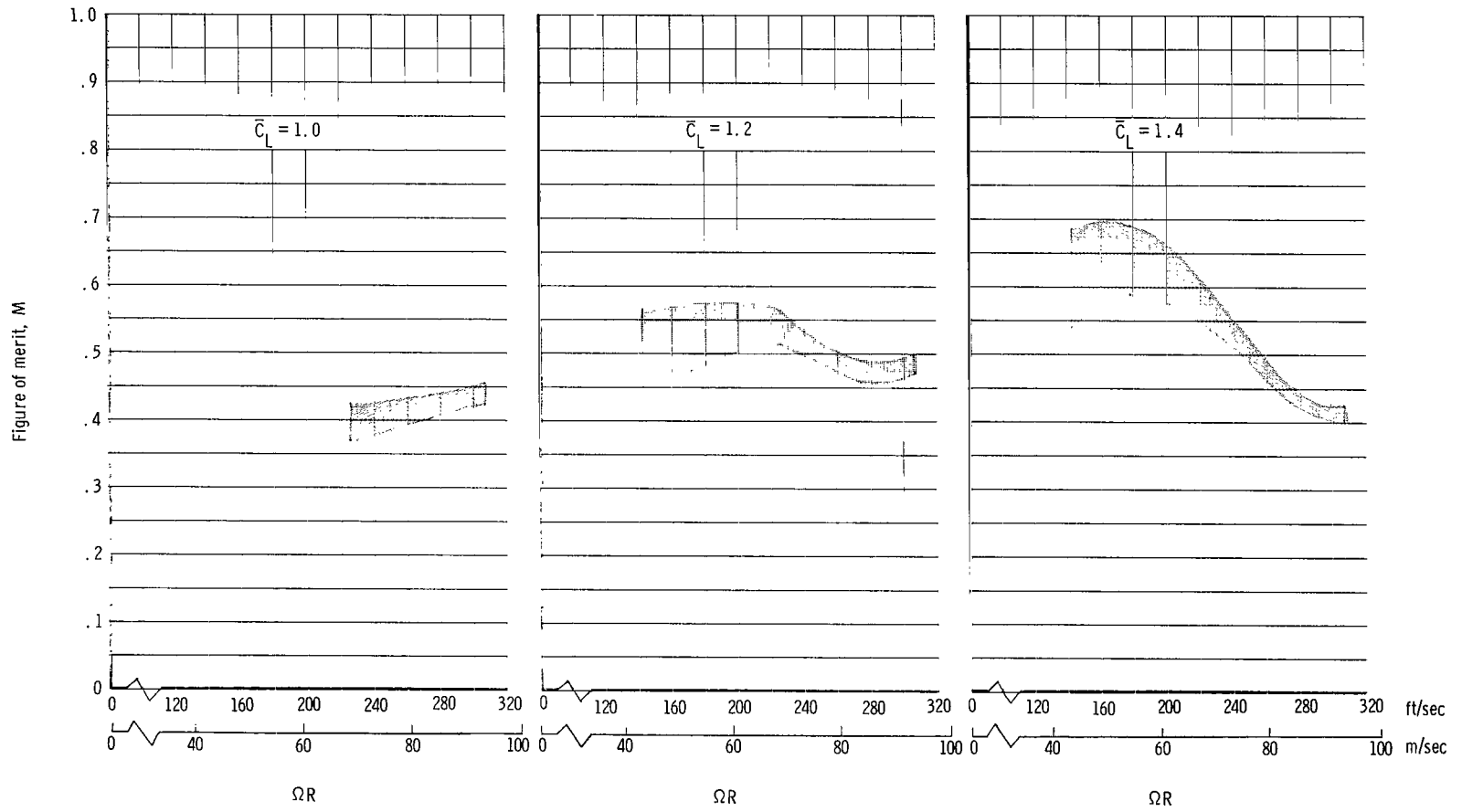
(a) Variation of thrust coefficient with tip speed.

Figure 13.- Effects of rotor tip speed on hovering characteristics of configuration 1. $i_s = -15^\circ$.



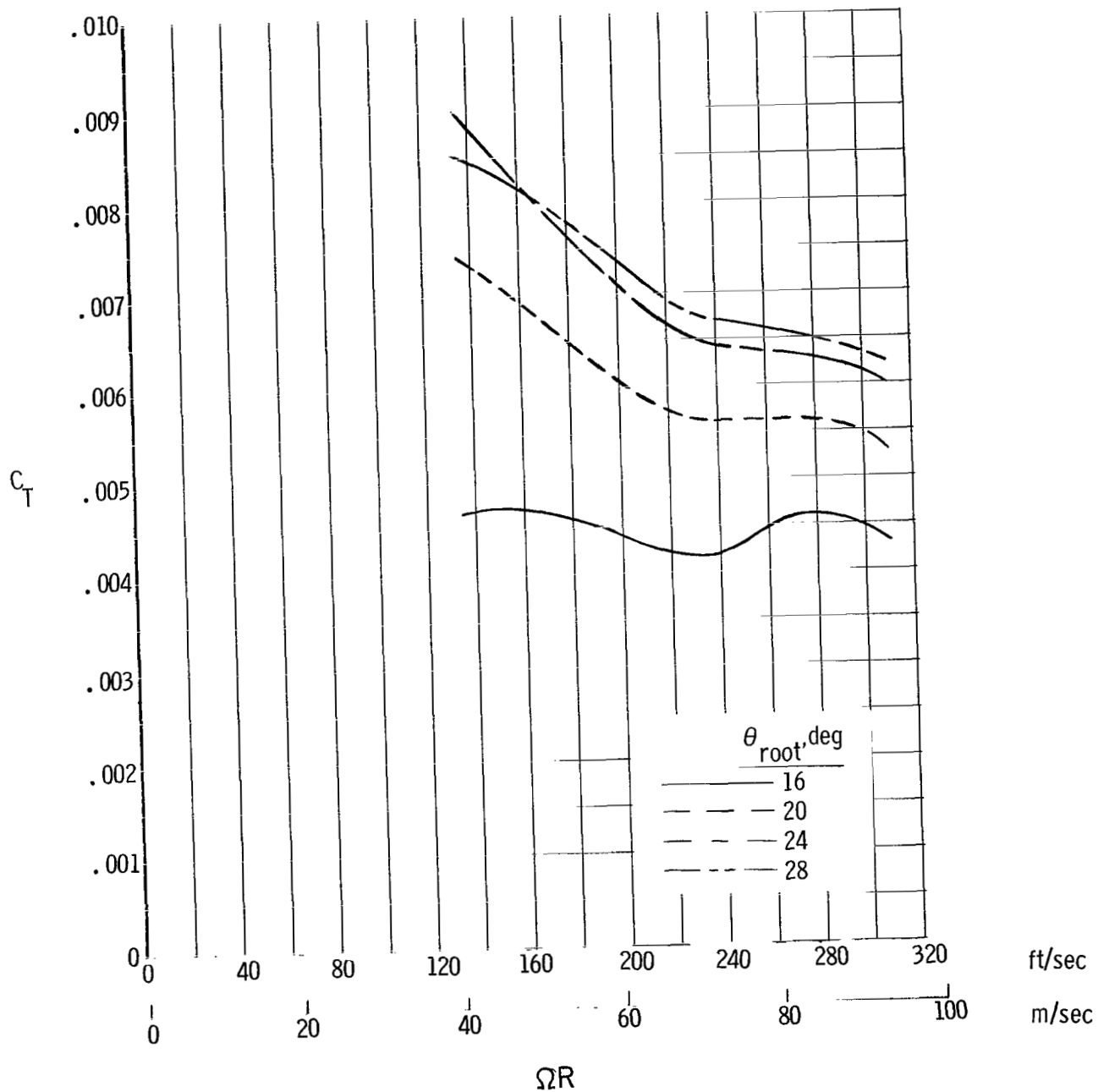
(b) Variation of torque-coefficient—solidity ratio with tip speed.

Figure 13.- Continued.



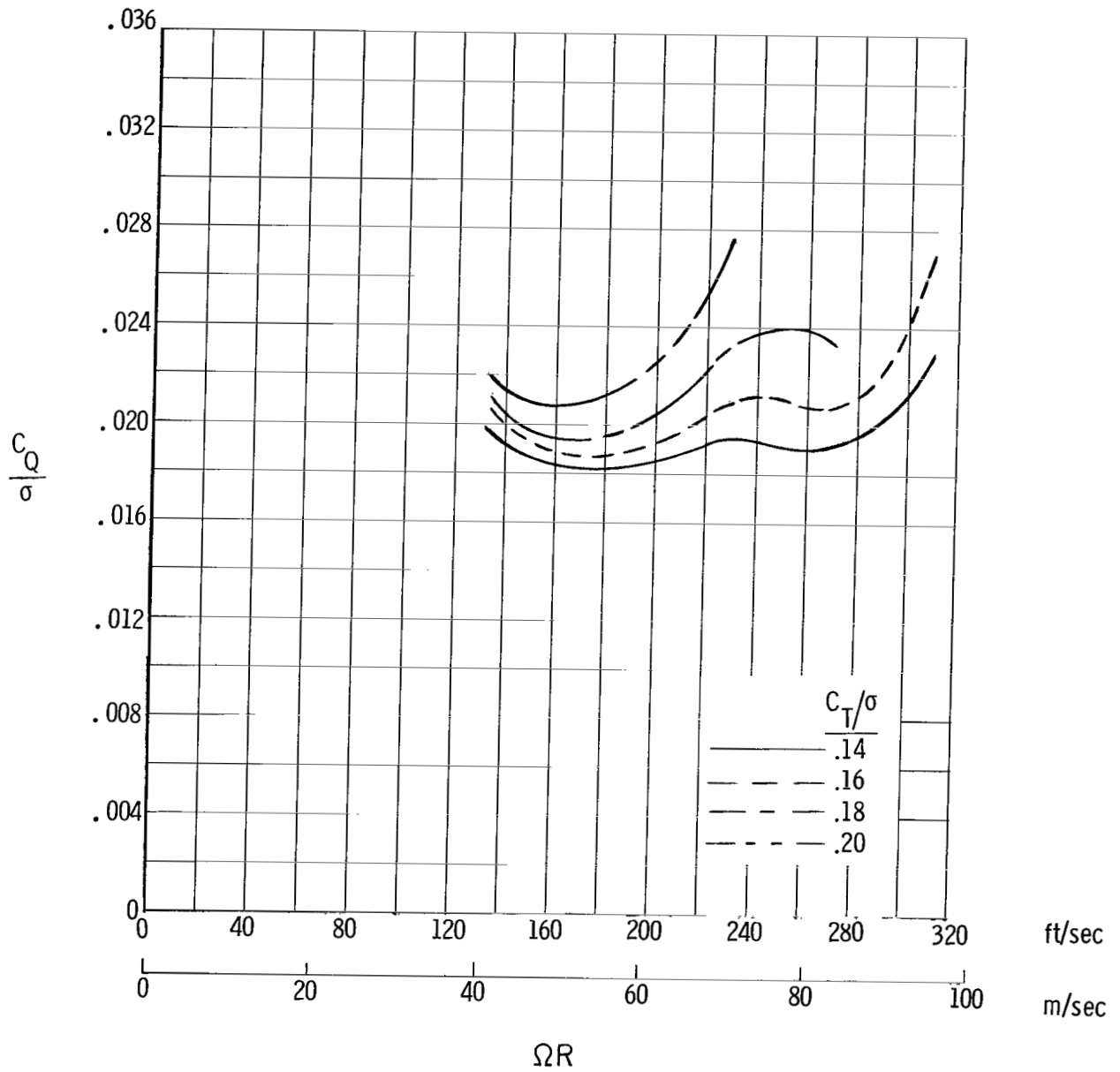
(c) Variation of rotor figure of merit with tip speed.

Figure 13.- Concluded.



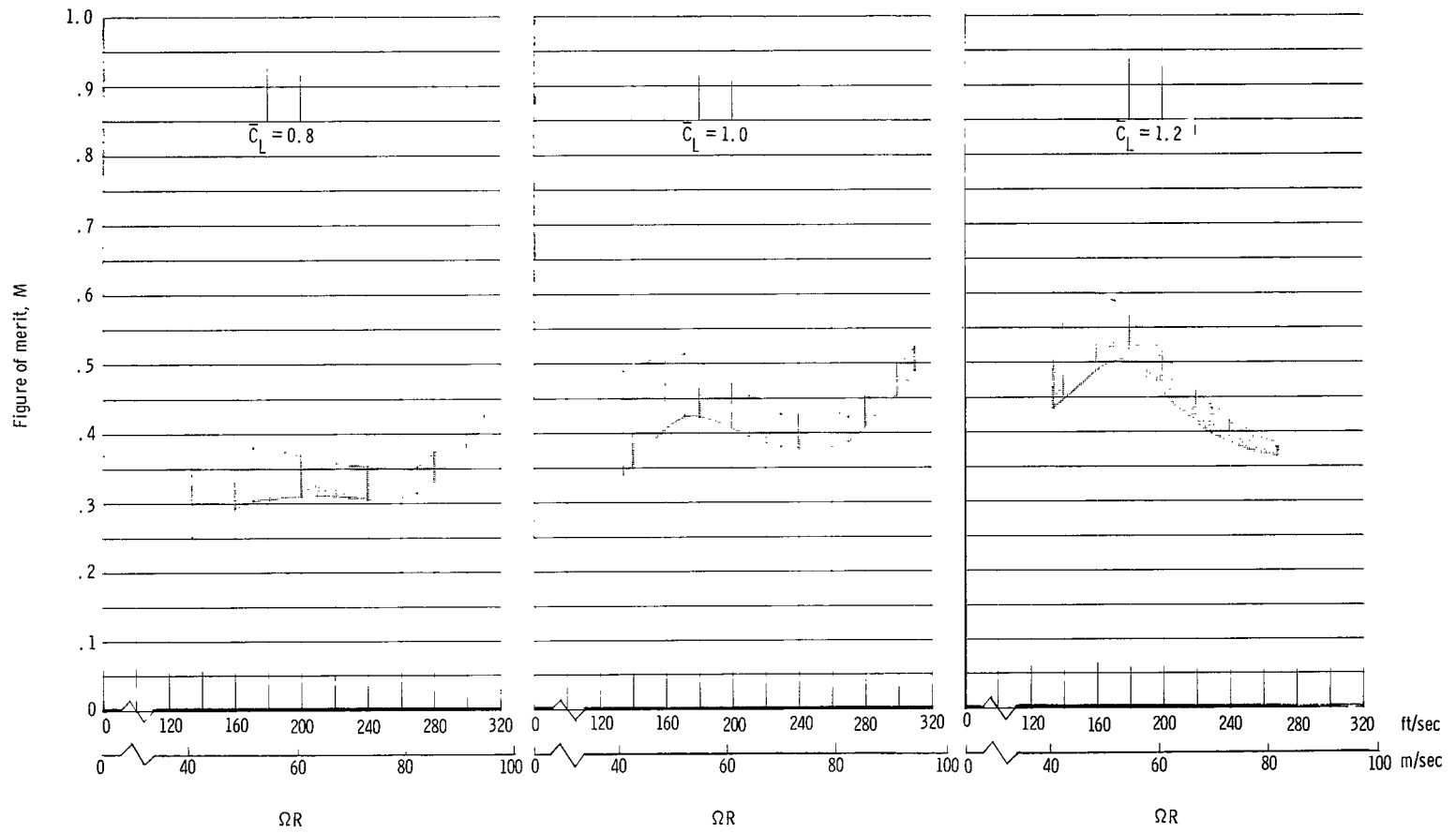
(a) Variation of thrust coefficient with tip speed.

Figure 14.- Effects of rotor tip speed on hovering characteristics of configuration 2. $i_s = -15^\circ$.



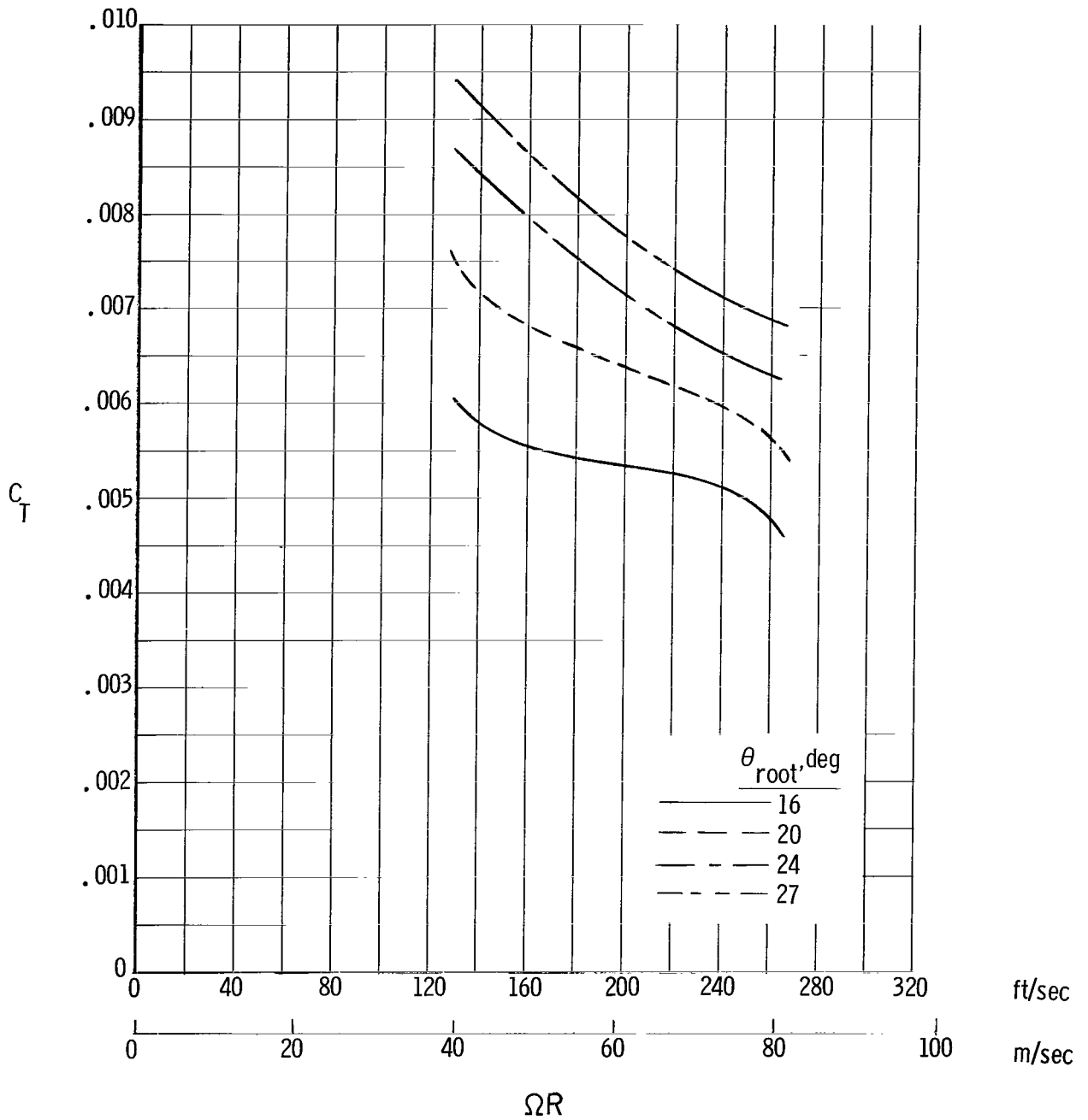
(b) Variation of torque-coefficient—solidity ratio with tip speed.

Figure 14.- Continued.



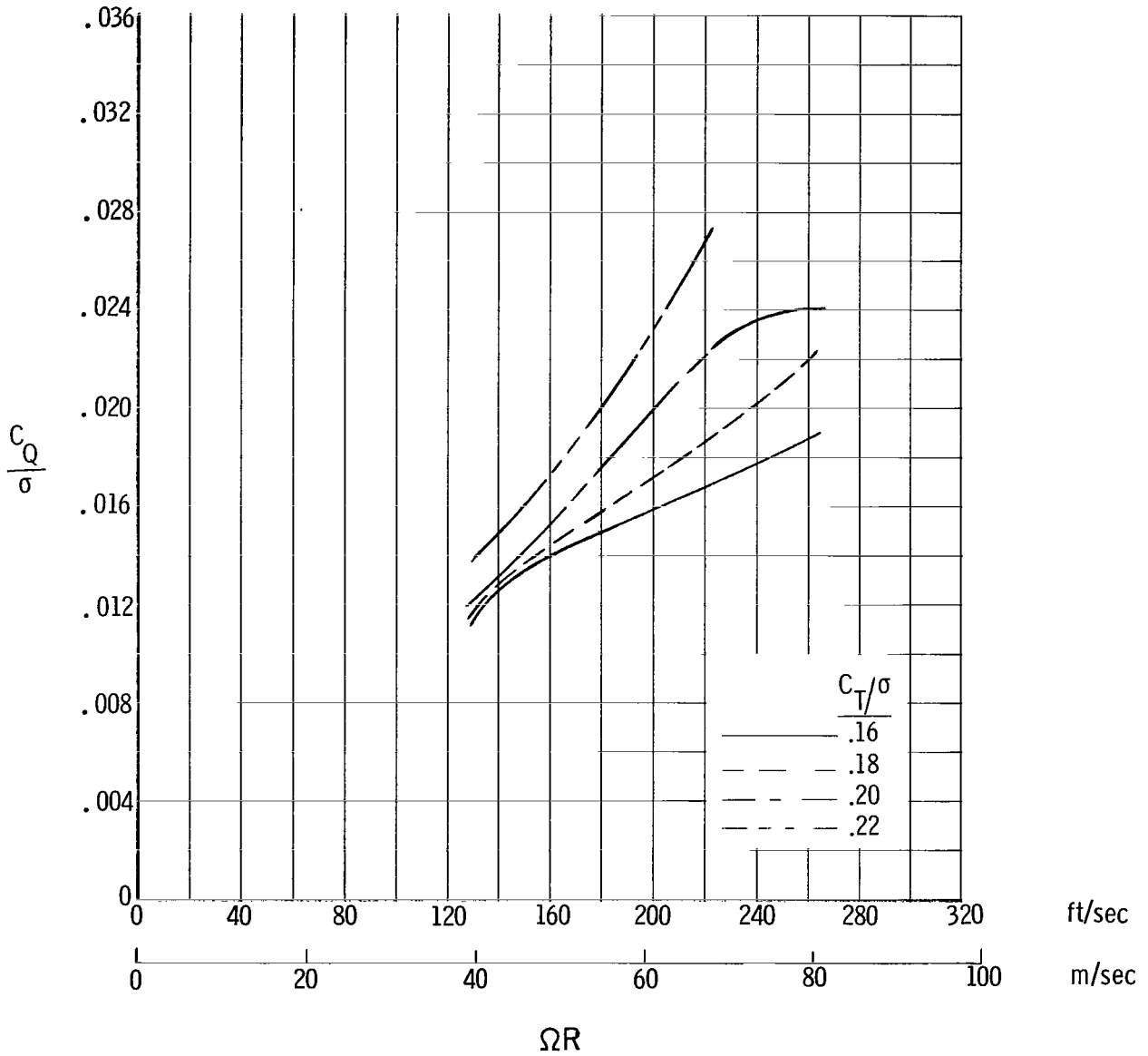
(c) Variation of rotor figure of merit with tip speed.

Figure 14.- Concluded.



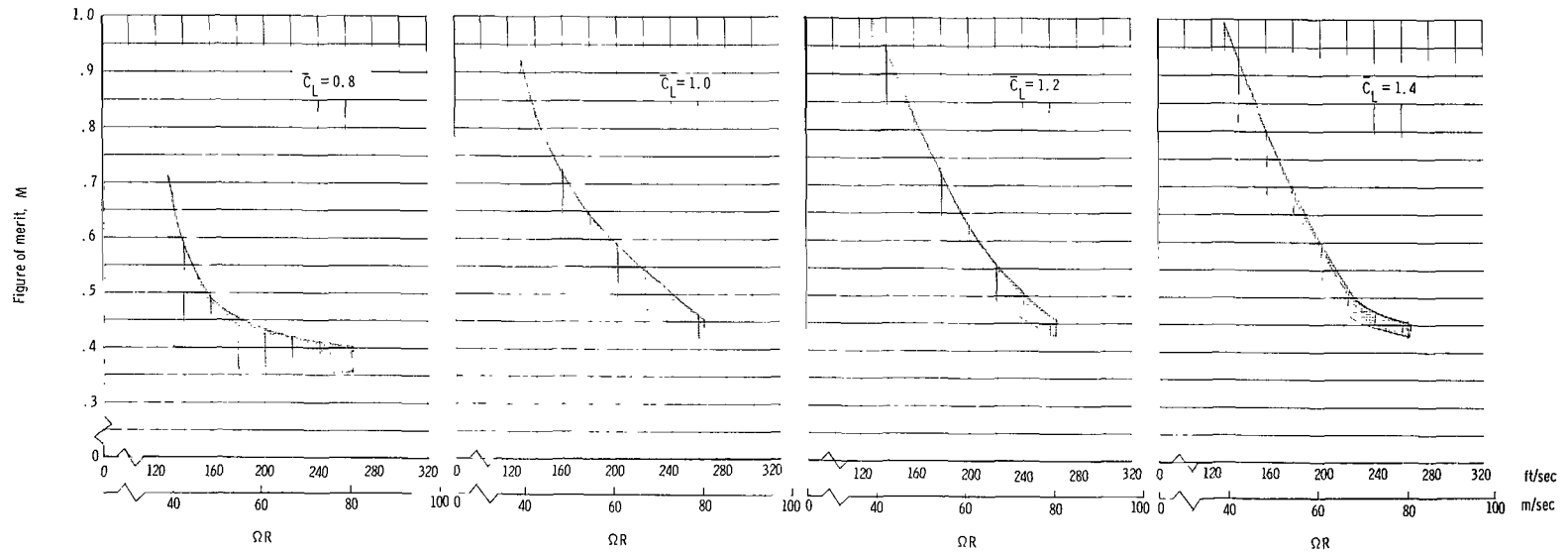
(a) Variation of thrust coefficient with tip speed.

Figure 15.- Effects of rotor tip speed on hovering characteristics of configuration 3. $i_s = -15^\circ$.



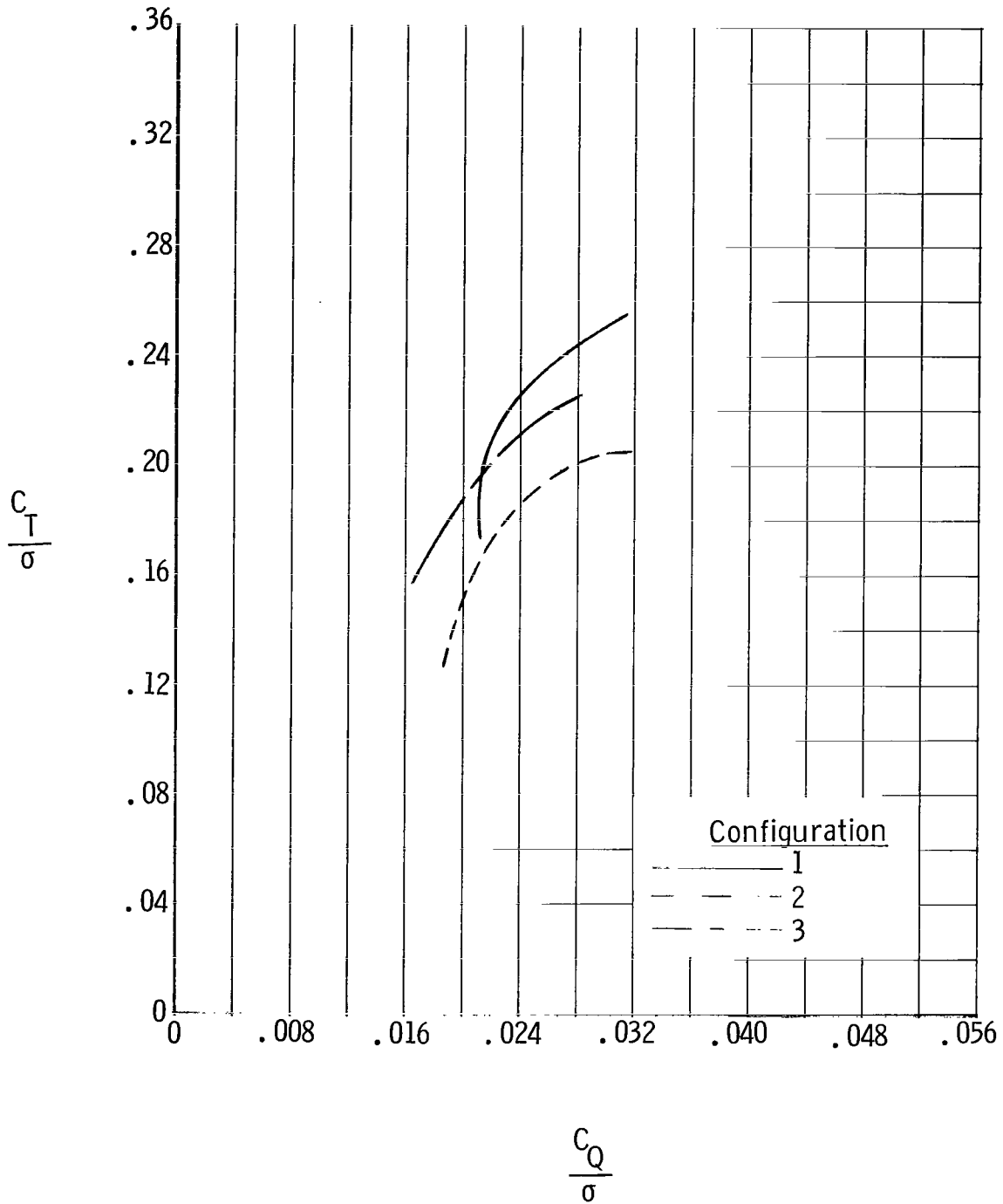
(b) Variation of torque-coefficient—solidity ratio with tip speed.

Figure 15.- Continued.



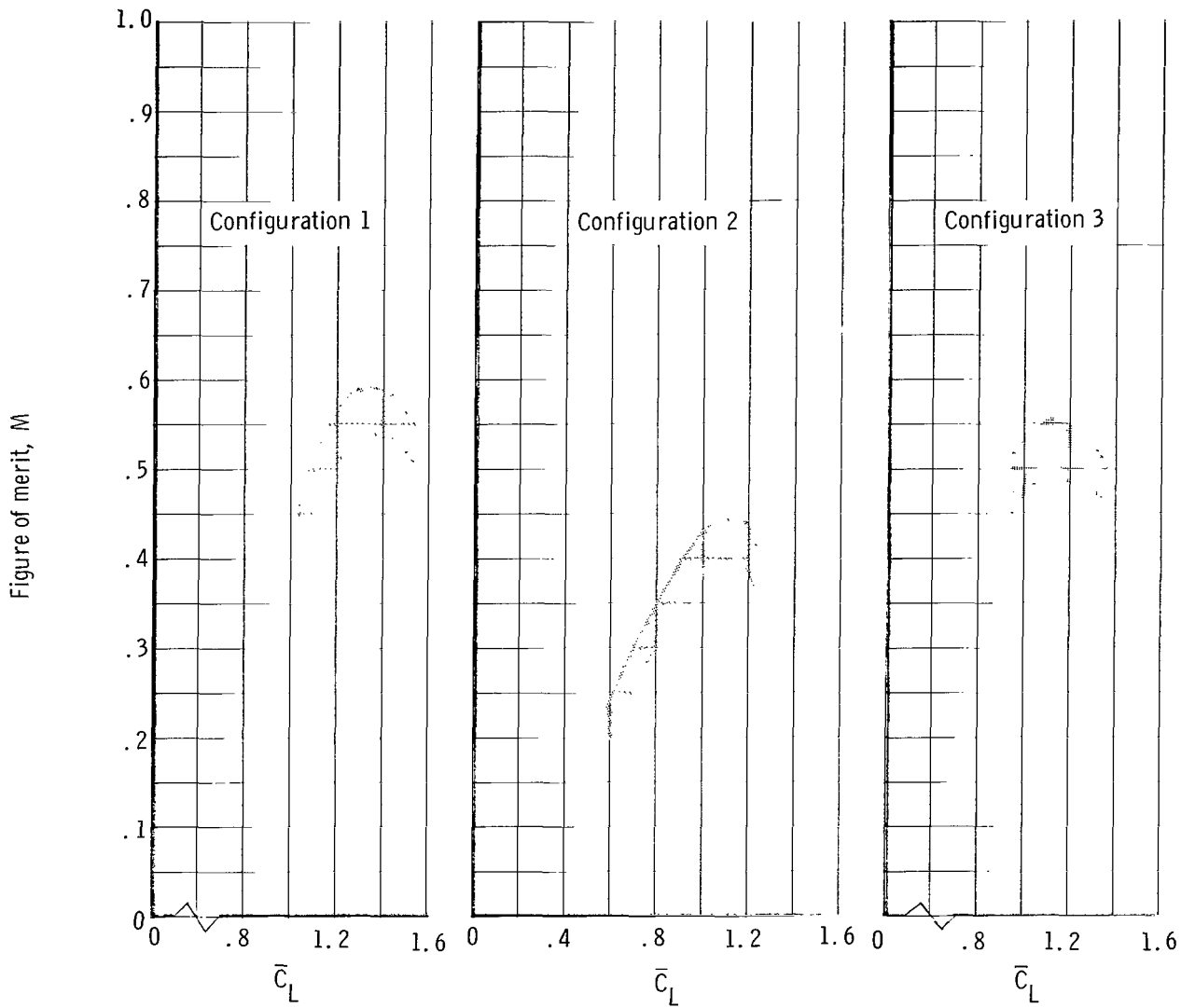
(c) Variation of rotor figure of merit with tip speed.

Figure 15.- Concluded.



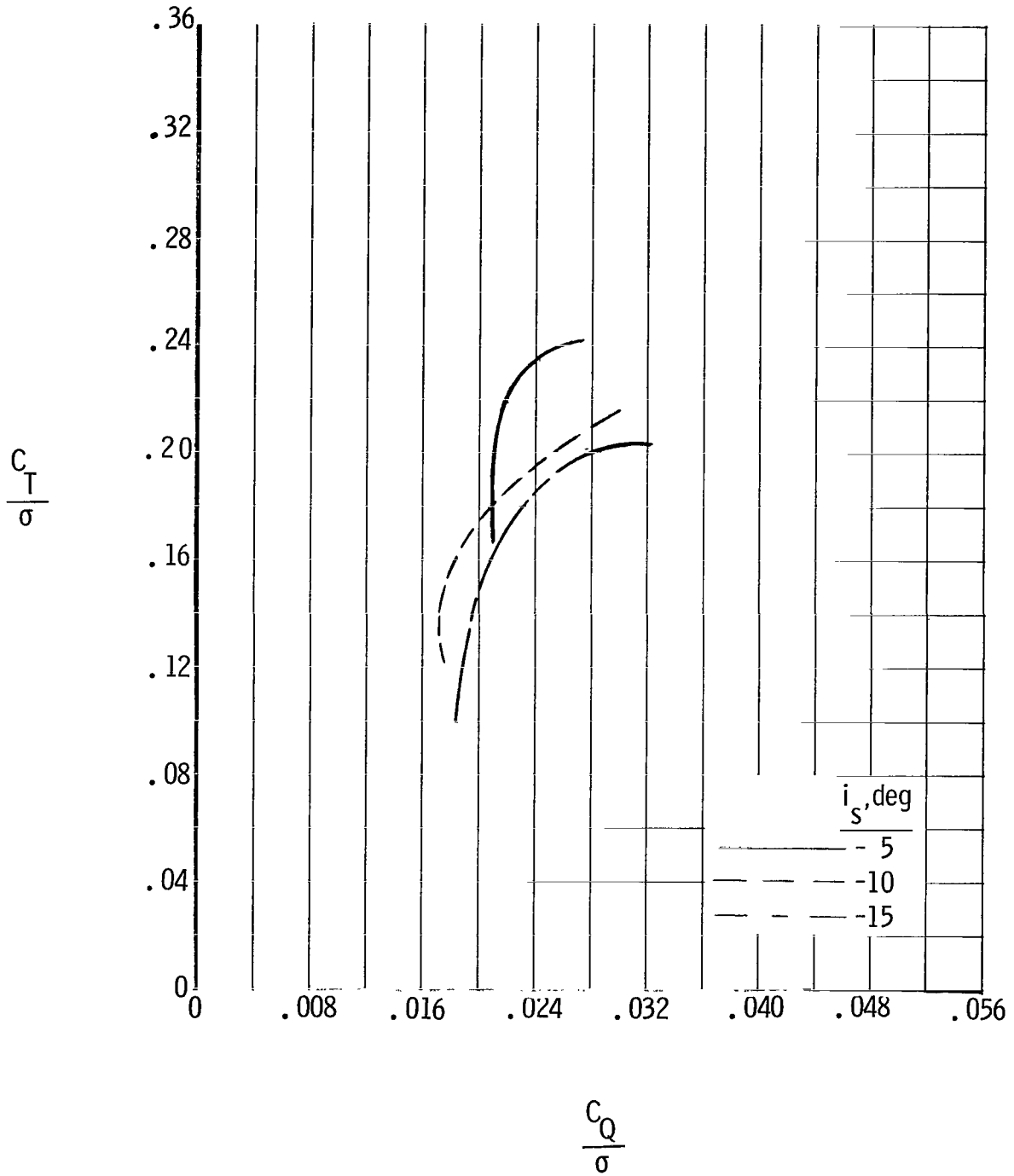
(a) Variation of thrust-coefficient—solidity ratio with torque-coefficient—solidity ratio.

Figure 16.- Effect of tip body mass and chordwise center of gravity. $i_s = -15^\circ$; $\Omega R = 220$ ft/sec (67 m/sec).



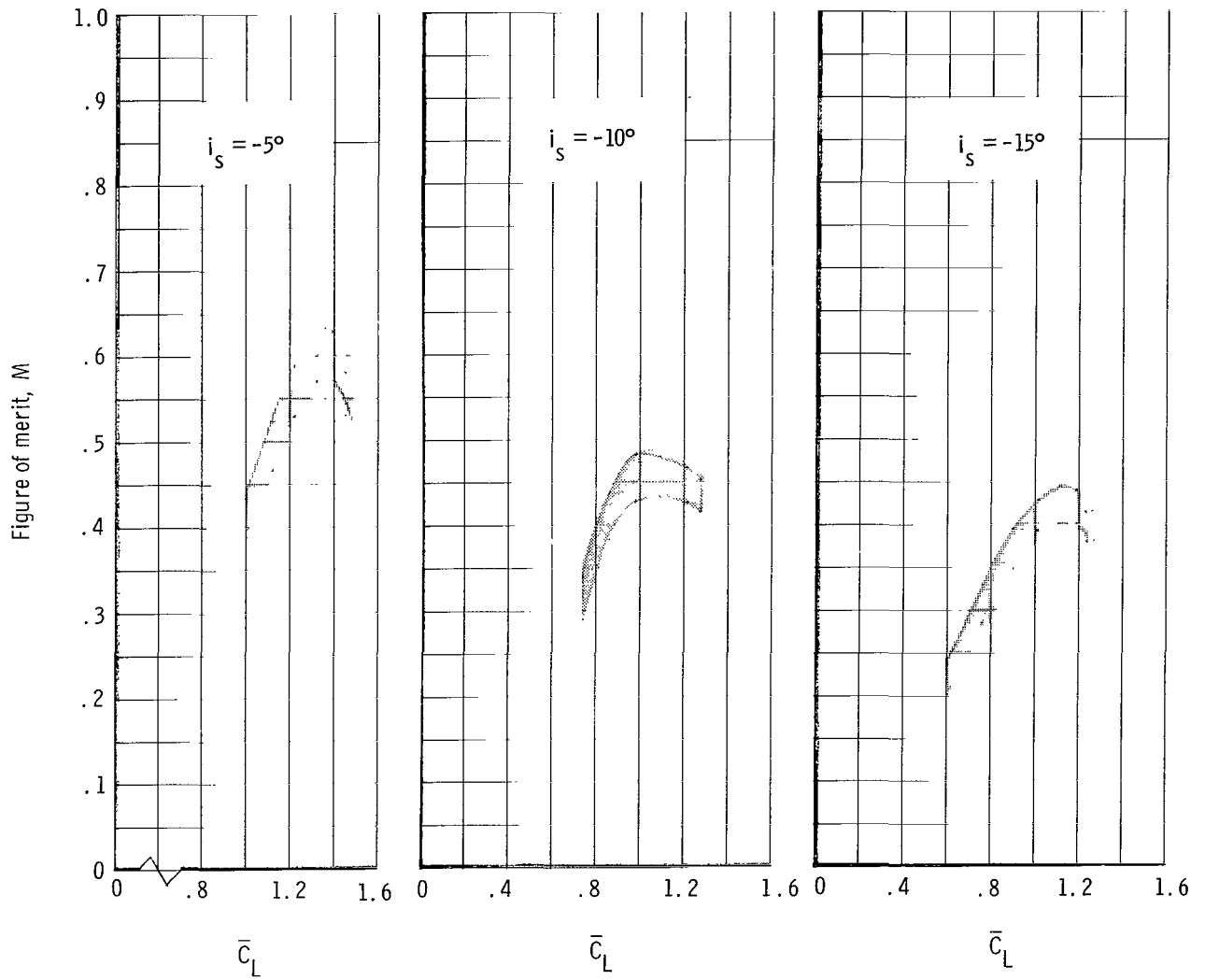
(b) Variation of rotor figure of merit with mean lift coefficient.

Figure 16.- Concluded.



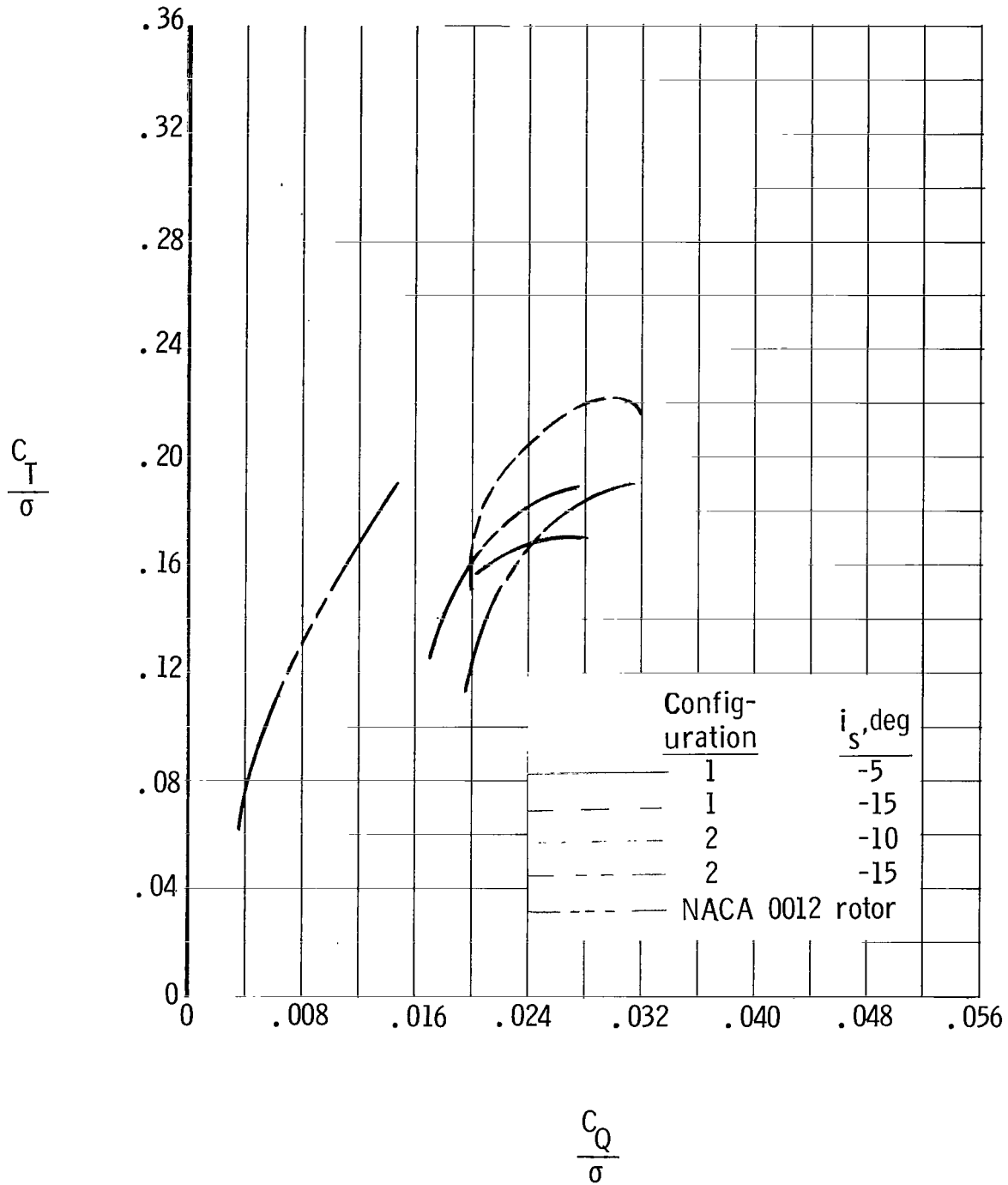
(a) Variation of thrust-coefficient—solidity ratio with torque-coefficient—solidity ratio.

Figure 17.- Effect of tip stabilizer incidence i_s on configuration 2. $\Omega R = 220$ ft/sec (67 m/sec).



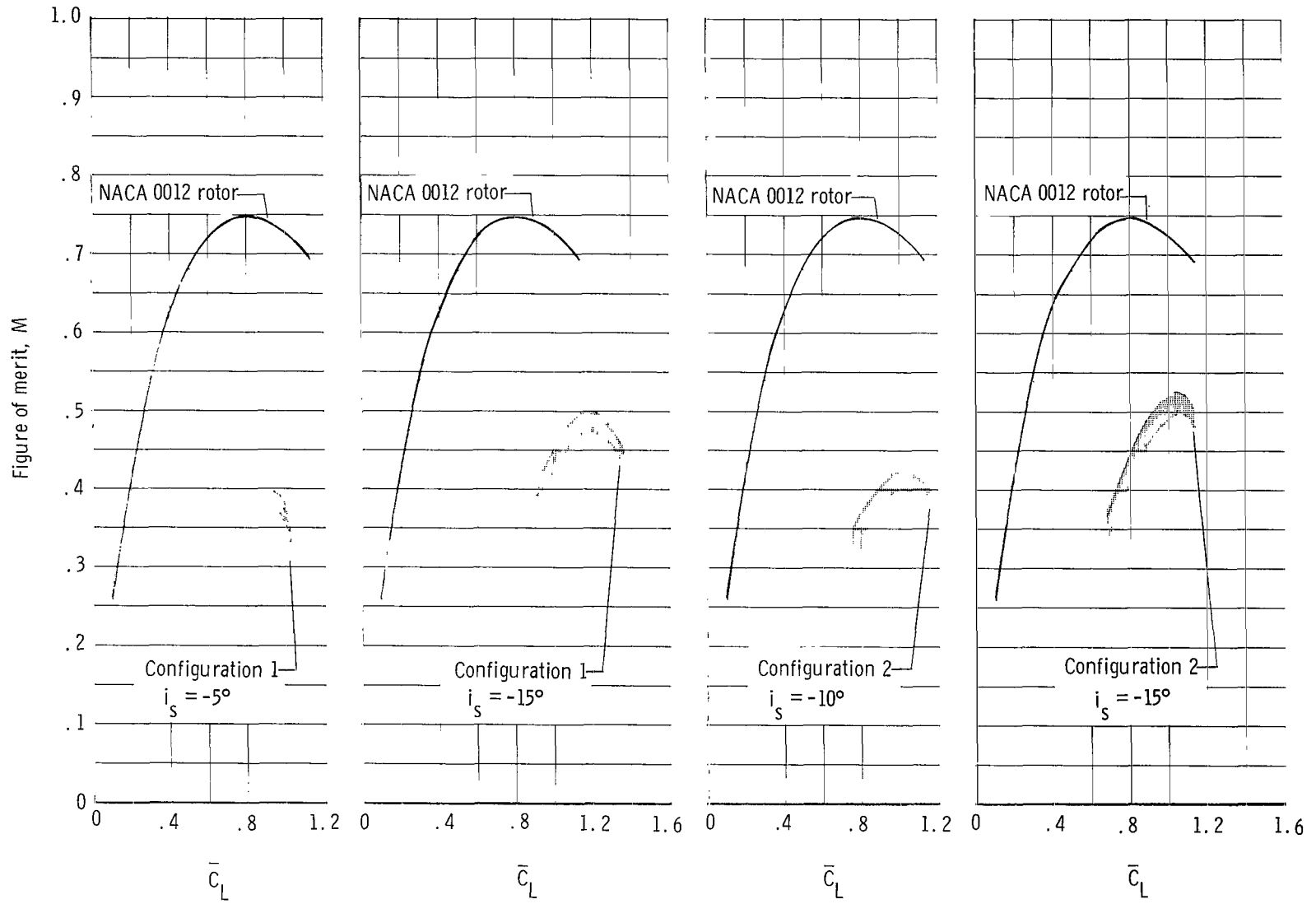
(b) Variation of rotor figure of merit with mean lift coefficient.

Figure 17.- Concluded.



(a) Variation of thrust-coefficient—solidity ratio with torque-coefficient—solidity ratio.

Figure 18.- Comparison of flexible rotor configuration with conventional rotor. $\Omega R = 310 \text{ ft/sec}$ (94.5 m/sec).



(b) Variation of rotor figure of merit with mean lift coefficient.

Figure 18.- Concluded.

FIRST CLASS MAIL

08274 00003
311 001 21 01 303
AFRICAN STATES LABORATORY/AFSL/

1960 AIR FORCE BASE, MEXICO 8711

POSTMASTER: If Undeliverable (Section 158
Postal Manual) Do Not Return

"The aeronautical and space activities of the United States shall be conducted so as to contribute . . . to the expansion of human knowledge of phenomena in the atmosphere and space. The Administration shall provide for the widest practicable and appropriate dissemination of information concerning its activities and the results thereof."

— NATIONAL AERONAUTICS AND SPACE ACT OF 1958

NASA SCIENTIFIC AND TECHNICAL PUBLICATIONS

TECHNICAL REPORTS: Scientific and technical information considered important, complete, and a lasting contribution to existing knowledge.

TECHNICAL NOTES: Information less broad in scope but nevertheless of importance as a contribution to existing knowledge.

TECHNICAL MEMORANDUMS: Information receiving limited distribution because of preliminary data, security classification, or other reasons.

CONTRACTOR REPORTS: Scientific and technical information generated under a NASA contract or grant and considered an important contribution to existing knowledge.

TECHNICAL TRANSLATIONS: Information published in a foreign language considered to merit NASA distribution in English.

SPECIAL PUBLICATIONS: Information derived from or of value to NASA activities. Publications include conference proceedings, monographs, data compilations, handbooks, sourcebooks, and special bibliographies.

TECHNOLOGY UTILIZATION PUBLICATIONS: Information on technology used by NASA that may be of particular interest in commercial and other non-aerospace applications. Publications include Tech Briefs, Technology Utilization Reports and Notes, and Technology Surveys.

Details on the availability of these publications may be obtained from:

SCIENTIFIC AND TECHNICAL INFORMATION DIVISION
NATIONAL AERONAUTICS AND SPACE ADMINISTRATION
Washington, D.C. 20546